M

LA-8862-MS, Revised

UNCL...

Los Alamos National Laboratory is operated by the University of California for the United States Department of Energy under contract W-7405-ENG-36.

Magnetic Switches and Circuits

DTIC QUALITY INSPECTED 4

PLEASE RETURN TO:

BMD TECHNICAL INFORMATION CENTER
BALLISTIC MISSILE DEFENSE ORGANIZATION
7100 DEFENSE PENTAGON
WASHINGTON D.C. 20301-7100

19980309 353

u 3357

Los Alamos
Los Alamos National Laboratory
Los Alamos, New Mexico 87545

UNCLASSIFIED

Edited by Jill Warren
Photocomposition by Kristine Mathieson
Assisted by Samia L. Davis

Accession Number: 3859

Publication Date: May 01, 1982

Title: Magnetic Switches and Circuits

Personal Author: Nunnally, W.C.

Corporate Author Or Publisher: Los Alamos National Laboratory, Los Alamos, NM 87545 Report Number: LA-8862-MS, Revised

Report Prepared for: U.S. Department of Energy Report Number Assigned by Contract Monitor: SLL 83-U-021

Comments on Document: Archive, RRI, DEW

Descriptors, Keywords: Magnetic Switch Circuit Pulse Compression Low Inductance Presaturation Material Parameter Couple Coefficient Stripline Transformer High Voltage Silicon Controlled Rectifier SCR Operation Tr

Pages: 00037

Cataloged Date: Nov 20, 1992

Document Type: HC

Number of Copies In Library: 000001

Record ID: 25141

Source of Document: DEW

Magnetic Switches and Circuits

W. C. Nunnally

Revised pages are 11, 17, 18, 19, 24, 28, 35, and 37.

NOMENCLATURE

	Symbols		Subscript Symbols
A	area	B	back
B	flux density	I	insulation
C	capacitor	L	lamination
DF	dimension factor	ME	magnetic element
DX	sections of width	SE	section
E	energy	T	total
F	factor	a	average
H	magnetic field	ap	applied
I	current	c	coercive force
J	section adjacent to center of lamination	e	eddy
K	coupling coefficient	f	front
KS	sign of the current derivative	g	group
L	inductance	i	initial
M	multiples	k	constant
N	number	m	magnetic material
O	outside	mag	magnetizing
P	power	max	maximum
R	resistance	min	minimum
S	series	n	to the nth degree
SF	stacking factor	o	free space
T	transfer or transformer	pri	primary
T_s	switching time	r	relative
V	voltage	rem	remnant
W	width	s	surface
X	depth into lamination	sat	saturated
$\dot{X}$	velocity	sec	secondary
d	differential	st	series path
f	fall	sw	switching
m	lamination group	t	turns
r	radius	w	winding
t	time	σ	surface
u	unit	λ	stray
w	waveform	ε	effective
x	thickness		
y	variable		
ℓ	magnetic field path length		
μ	permeability		
α	fraction		
σ	magnetic skin depth		
$\triangle$	changing value		
ρ	material resistivity		
$\emptyset$	magnetic flux		
τ	time		
τ_r	risetime		
ω	sinusoidal frequency		

MAGNETIC SWITCHES AND CIRCUITS

by

W. C. Nunnally

ABSTRACT

This report outlines the use of saturable inductors as switches in lumped-element, magnetic-pulse compression circuits. The operation of the three basic types of magnetic pulse compression circuits is discussed and the characteristic use of each is defined. In addition, the geometric constraints and magnetic pulse compression circuits used in short-pulse, low-inductance systems are considered. The scaling of presaturation leakage currents, magnetic energy losses, and switching times with geometrical and material parameters are developed to aid in evaluating magnetic pulse compression systems in a particular application. Finally, a scheme for increasing the coupling coefficient in saturable stripline transformers is proposed to enable their use in the short-pulse, high-voltage regime.

I. INTRODUCTION

The nonlinear characteristics of magnetic materials have been used in magnetic amplifiers for many years. More recently, magnetic switches and systems have been used in conjunction with solid-state switches [silicon controlled rectifiers (SCR)] to develop high-reliability, long-life radar modulators with pulse widths in the 1- to 10-μs range.[1-3] The advantages of magnetic switches and systems warrant extending this technology to the higher voltages (50-500 kV) and shorter pulse widths (50-500 ns) required by present and projected laser and accelerator systems. This report identifies the areas in which circuit designs and geometry must be modified and areas in which magnetic materials and fabrication techniques must be developed to permit operation of magnetic switches and systems in the range required by short-pulse, high-voltage laser and accelerator systems.

The magnetic geometries discussed in this report are made from thin tapes of various steel alloys commonly used for high frequency applications. Ferrite materials can be used in magnetic switching applications, but the much larger saturation flux density of the steel alloys, in general, permits switching larger voltages with a smaller volume of magnetic material than do the ferrite materials.

II. OPERATION OF CIRCUITS USING MAGNETIC SWITCHES

In conventional pulse power conditioning circuits and systems, the output pulse energy is transferred from a power supply to an intermediate energy storage device through a conventional switch then to the

load through another switch. The time required to charge the intermediate energy store is long compared to the output pulse length. Several stages of intermediate energy storage can be used between the power supply and the final output stage. The required output pulse energy is transferred in shorter and shorter periods of time so the instantaneous power is increased because the transfer time is decreased.

To minimize cost, complexity, reliability and switch energy losses, the number of transfer or time compression stages is usually minimized. The magnetic switch circuits generally use the same procedure using several sequential stages of resonant energy transfer to obtain pulse compression.

A. Basic Resonant Energy Transfer

Most repetitive power conditioning systems use a resonant charge or resonant energy transfer circuit [Fig. 1(a)]. A power supply charges capacitor C1 to voltage V_{max}. The energy stored in capacitor C1 is resonantly transferred to capacitor C2 through the inductance L by closing the switch at time $t = 0$. The result is a sinusoidal current that, in the absence of resistive losses, is given by

$$I(t) = I_m \sin \omega t \quad , \tag{1}$$

where

$$\omega = \left(\frac{1}{L_T C_T} \right)^{1/2}$$

L_T is the total circuit inductance, and C_T is the total series capacitance given by

$$C_T = \frac{C1 \cdot C2}{C1 + C2} \tag{2}$$

The peak current is given by

$$I_{max} = V_{max} \left(\frac{C_T}{L_T} \right)^{1/2} \tag{3}$$

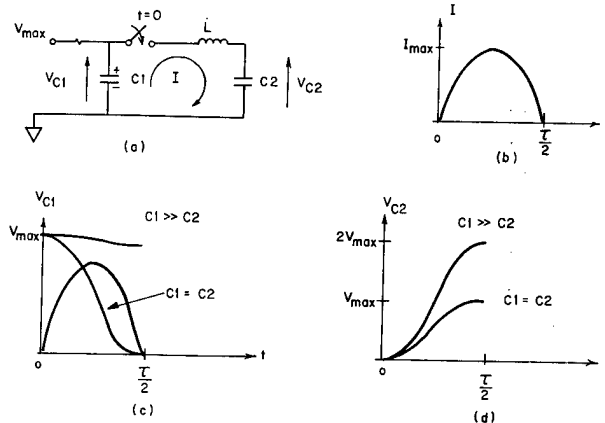and the voltages on C1 and C2 are respectively

Fig. 1.
Basic resonant energy transfer circuit and waveforms.

2

$$V_{C1}(t) = V_{max} \left[1 - \frac{C2}{C1 + C2}(1 - \cos \omega t) \right] \qquad (4)$$

and

$$V_{C2}(t) = V_{max} \left[\frac{C2}{C1 + C2}(1 - \cos \omega t) \right] \quad . \qquad (5)$$

The resonant time T for the transfer circuit is given by

$$\frac{T}{2} = \pi (L_T C_T)^{1/2} \qquad (6)$$

Another important characteristic of this circuit is the maximum energy transfer ET given by

$$ET = \int_0^{T/2} I(t)V(t)dt \quad . \qquad (7)$$

Using Eq. (6)

$$C_T = \frac{1}{L_T} \left(\frac{T}{2\pi} \right)^2 \quad . \qquad (8)$$

Using Eq. (3)

$$I_m = \frac{V_{max}T}{2\pi L_T} \qquad (9)$$

so that Eq. (7) becomes

$$ET = \frac{V_{max}(T)}{2\pi LT} \int_0^{\pi/\omega} \sin \omega t \, (1 - \cos \omega t)dt \qquad (10)$$

or

$$ET = \left(\frac{V_{max}T}{2\pi} \right)^2 \frac{1}{L_T} \quad . \qquad (11)$$

Three important features of resonant energy transfer are illustrated by the waveforms of Fig. 1(c) and (d). First, without resistive losses, 100% energy transfer from capacitor C1 to capacitor C2 is possible if C1 = C2. Second, if C1 $\gg$ C2, the peak voltage on C2 approaches twice that originally on C1. Finally, if C1 = C2, the voltage across and current through the switch, which assist in commutating or opening the solid-state or thyratron switches, are both zero. Thus, energy is prevented from returning to C1.

3

B. Low Inductance Saturable Inductor Design

The most important point of the resonant energy transfer circuit discussion from Eq. (11) is that L_T cannot be exceeded to transfer E_T at V_{max} in time $T/2$. The inductance of one or more magnetic elements is a major portion of the total inductance, so each part must be designed with an even smaller maximum inductance to operate in the circuit. A general form for inductance is given in Eq. (12).

$$L = \frac{\mu_o \mu_r A_T N^2}{\ell} \quad , \tag{12}$$

where μ_o and μ_r are the free space and relative permeability, respectively, N is the number of conductor turns, and ℓ is the magnetic field path length. The total cross-section area A_T is determined principally by the required flux content or volt-seconds of the magnetic material in the core derived from flux conservation or

$$\frac{1}{N_t} \int_0^{T_{sat}} V(t)dt = \int_{A_m} \overline{B} \cdot \overline{ds} \quad , \tag{13}$$

where N_T is the number of conductor turns around the magnetic material.

In Eq. (13) V(t) is the voltage applied across the saturable inductor before saturation between $t = 0$ and $t = T_{sat}$. The right side of Eq. (13) is the flux in the magnetic material and is usually approximated by

$$\int_{A_m} \overline{B} \cdot \overline{ds} = \triangle B A_m \quad , \tag{14}$$

where $\triangle B$ is the magnetic flux density change or swing and A_m is the magnetic material cross-section area. To minimize A_m, $\triangle B$ is usually made as large as possible by biasing the magnetic material into reverse saturation so $\triangle B = 2B_s$. The stacking factor SF relates A_T to A_m by

$$SF \triangleq \frac{A_m}{A_T} = \frac{A_m}{A_I + A_m} = \frac{x_L}{x_I + x_L} \quad , \tag{15}$$

where A_I is the cross-section area of the insulation required between magnetic laminations as discussed below.

Using ferrite materials with approximately one-third the saturation flux density of steel material requires three times the cross-section area to support the same voltage for the same period. Equation (12) implies that the magnetic path length for a similar inductance using ferrite materials would also be three times as large. Thus, approximately nine times more magnetic material volume is required when ferrite materials are used than when steel materials are used. The inductance of a magnetic element can be written

$$L_{ME} = \alpha L_T = \alpha \frac{\mu_o \mu_r N_T}{SF \ell 2 B_{sat}} \int_0^T V(t)dt \quad , \tag{16}$$

where α is the fraction, < 1, of L_T represented by the magnetic element. For a saturable inductor subjected to a constant voltage before transfer for a time T_{sat}, $V(t) = V_{max}$ and the saturated inductance of the magnetic element becomes

$$L_{ME} = \frac{\alpha \mu_o \mu_s A_T N^2 \ V_{max} T_{sat}}{SF \ell_{sat} 2 B_s} \quad . \tag{17}$$

4

Because N_T is limited to a maximum of two in extremely low-inductance circuits, the only free parameter is the saturated magnetic path length, ℓ_{sat}. For a completely saturated element, the magnetic path length is approximately equal to the winding width. Thus, increasing the conductor width is the only means of obtaining the small inductances required for high-energy, short-pulse magnetic pulse compressors.

The low-inductance geometry of two saturable inductors (Fig. 2) is identical to that required for low-transmission line impedance, compatible with the large currents and voltages required for this experiment. The stripline saturable inductor of Fig. 2(a) can become a triplate stripline if a top ground conductor is added. The type of inductor geometry is determined by the load geometry and chosen so minimum total inductance results.

C. Series Magnetic Pulse Compressor

The circuits that use magnetic switches also use multiple, successive resonant energy-transfer circuits. Thus, the energy transferred in T/2 at maximum voltage V_{max} is inversely proportional to the total circuit inductance L_T.

A basic series magnetic pulse compressor, sometimes called a Melville[1] line circuit, (Fig. 3) uses a conventional initial SCR thyratron, spark gap, etc., but the current requirements are reduced because of the long initial current conduction times. Saturable inductors or magnetic switches in each mesh are designed with a flux content to saturate when the capacitor immediately ahead is charged to V_{max}.

A series magnetic pulse compressor with current gain and pulse compression (Fig. 4) achieves pulse compression by decreasing the resonant time of each successive mesh by decreasing the saturated inductance in that stage. For equal capacitor values in each stage, without resistive losses, the voltage on the final stage is equal to the initial voltage so the energy transfer efficiency to the load is 100%.

In contrast, a series magnetic pulse compressor with voltage gain (Fig. 5) achieves voltage gain of two per stage by making each successive capacitor much smaller than the previous stage. This arrangement also reduces the resonant time of each successive mesh causing pulse compression, but the energy transfer from input to output is very low. Thus, a series magnetic pulse compressor with good energy transfer efficiency compresses the input pulse in time at constant voltage.
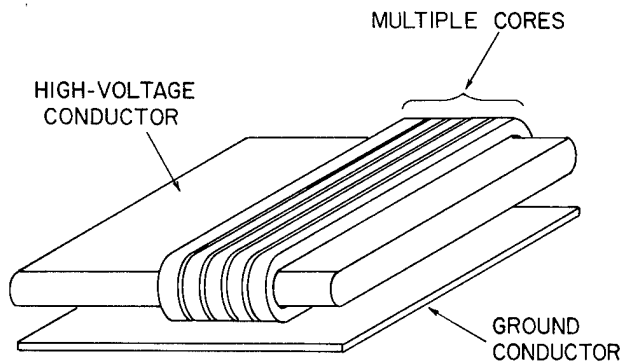

Fig. 2(a).

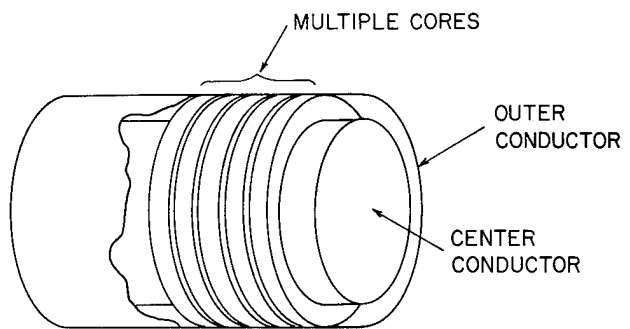Low-inductance stripline saturable inductor.

Fig. 2(b).

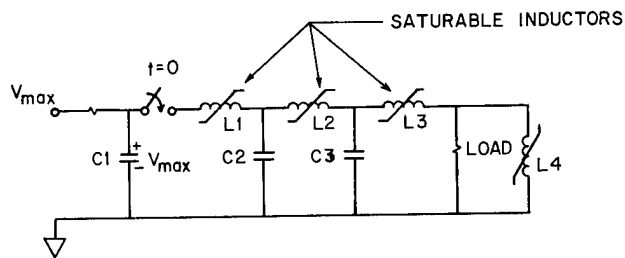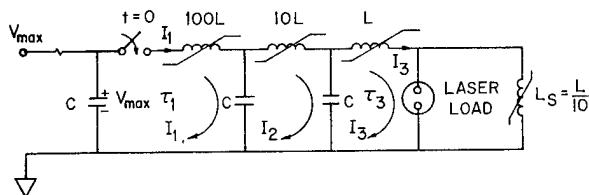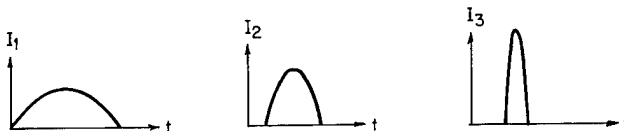Low-inductance coaxial saturable inductor.

Fig. 3.
Basic 3-stage series magnetic pulse compressor.

$$\text{CURRENT GAIN} = \frac{I_3}{I_1} = (50)^{1/2} \simeq 7$$

$$\text{PULSE COMPRESSION} = \frac{\tau_1}{\tau_3} = (50)^{1/2} \simeq 7$$

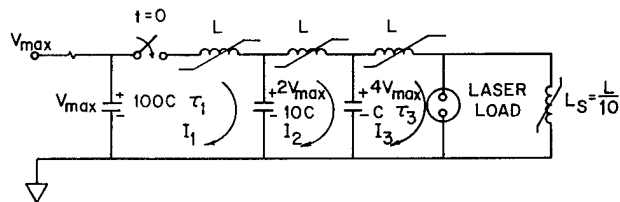$$\text{ENERGY TRANSFER EFFICIENCY} = \frac{\epsilon_3}{\epsilon_1} \simeq 1.0$$

Fig. 4.
Series magnetic pulse compressor with current gain.

D. Parallel Magnetic Pulse Compressor

In the parallel magnetic pulse compressor circuit (Fig. 6), the magnetic switches are in parallel along the path of the energy transfer. The transformers are the switching elements, which can also provide voltage gain or impedance matching. The transformer, which is the critical element of this circuit, requires

Fig. 6.
Basic 3-stage parallel magnetic pulse compressor.
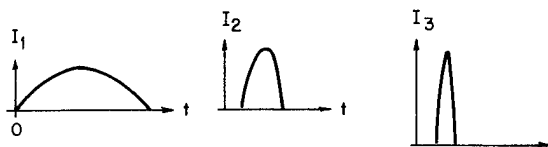
$$\text{VOLTAGE GAIN} = 4$$

$$\text{PULSE COMPRESSION} = \frac{\tau_1}{\tau_3} = (50)^{1/2} \simeq 7$$

$$\text{ENERGY TRANSFER EFFICIENCY}$$

$$\simeq \frac{\epsilon_3}{\epsilon_1} = \frac{8}{50} \simeq 0.16$$

Fig. 5.
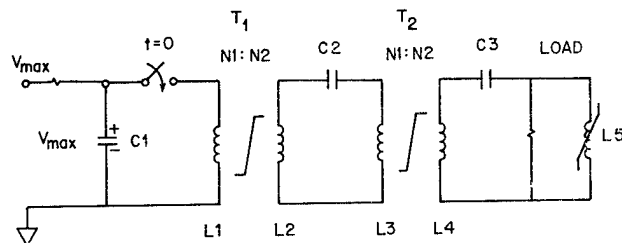Series magnetic pulse compressor with voltage gain.

much more innovation and understanding if experimenters are to design a high-voltage, short-pulse compressor.

The transformers of Fig. 6 are initially biased into reverse saturation. The energy transfer and pulse compression begin by closing the primary switch at t = 0. Current flows from C1, initially charged to V_{max}, through the primary of transformer T_1, forcing the magnetic core out of saturation and transferring the energy of C1 to C2. The flux content of T1 is designed so the magnetic material saturates at the end of the resonant energy transfer from C1 to C2 or at the half period of the oscillation. During the energy transfer from C1 to C2 through T_1, T_2 is biased to reverse saturation. The current charging C2 is in the same direction as the initial reverse bias current so T_2 remains saturated and subsequent stages are not coupled to the transfer transient from C1 to C2. The saturation of T1 causes the secondary voltage of T_1 (acting as a switch) to fall to zero. The secondary current of T_1 reverses and having previously opposed the primary current in saturation, now increases the saturated drive. The reversing current now unsaturates T_2 to transfer the energy in C2 to capacitor C3 in a similar manner. In Fig. 6, L5 is placed across the load and is initially reverse biased. As the charging current for C3 flows through L5 in the same direction as the initial reverse bias current, the load is shorted during the charge of C3. When the secondary of T_2 saturates and the secondary current of T_3 reverses, L5 is driven out of saturation, and the voltage is then applied to the load. If the load is low impedance and the charging current can flow through the load before it flows through the main pulse, L5 may not be required.

The main advantage of the parallel magnetic pulse compressor is the voltage level shift provided by the transformer. This advantage is balanced by the additional complexity of the transformer design. The lossless energy transfer efficiency of the parallel magnetic pulse compressor can be perfect if the stage capacitors are designed to store the same energy as the previous stage but at the shifted voltage level. Figure 7 shows a three-stage parallel magnetic pulse compressor with voltage gain and total energy transfer. Because the capacitance of subsequent stages is decreased, the pulse width is also decreased to compress the transferred energy in time.

E. Transmission Line Magnetic Pulse Compressor

A third circuit using magnetic switches, the transmission line magnetic pulse compressor shown in Fig. 8, shapes the output pulse and compresses the energy transfer time. This circuit can be thought of as a modification of the series magnetic pulse compressor (Fig. 3) with the addition of pulse shaping.

VOLTAGE GAIN = 4
PULSE COMPRESSION = 4
ENERGY TRANSFER EFFICIENCY $\simeq \dfrac{\epsilon_3}{\epsilon_1} \times 100 \simeq 100\%$
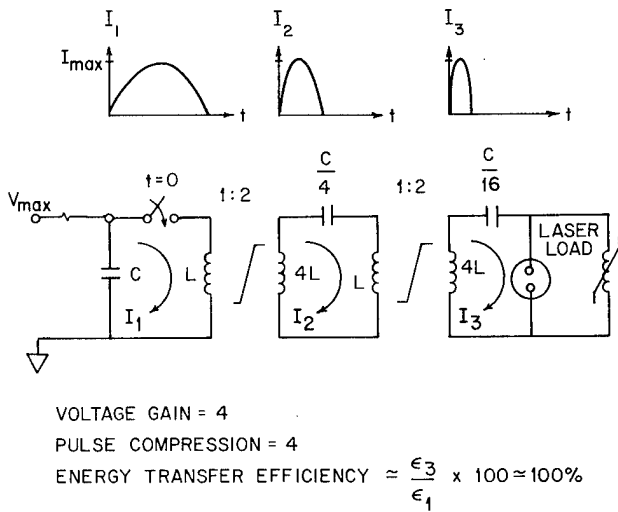
Fig. 7.
Parallel magnetic compressor with voltage gain.

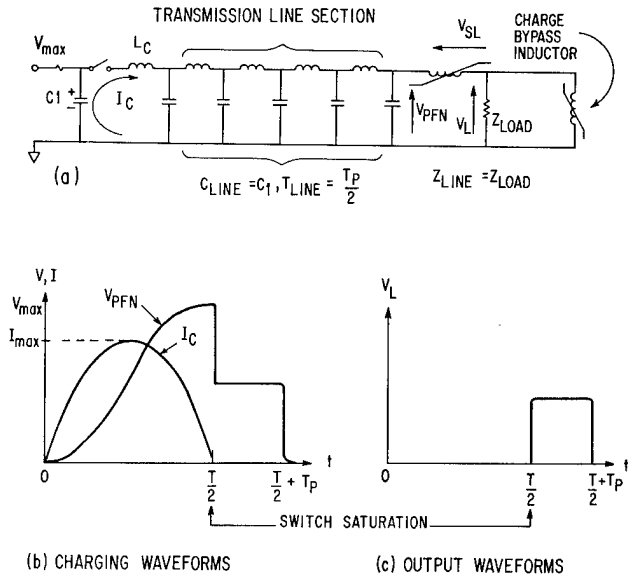(b) CHARGING WAVEFORMS   (c) OUTPUT WAVEFORMS

Fig. 8.
Transmission line magnetic pulse compressor.

7

F. Circuit Observations

Several conclusions should be drawn from the previous discussion of circuits using magnetic switches. First, the most straightforward method of using magnetic switches is the series or transmission line magnetic pulse compressor. However, to obtain high energy transfer efficiency, this system sacrifices voltage gain. The primary switch, which must be conventional, operates at the output voltage but at reduced current and switching requirements. On the other hand, the parallel magnetic pulse compressor can provide voltage gain at high-energy transfer efficiencies but requires the development of a low-inductance saturable transformer switch. The parallel magnetic pulse compressor scheme allows the possibility of using low-voltage, solid-state primary switches at high currents to obtain a solid-state system (semiconductor and magnetic) that provides the required reliability and lifetime for many applications. Thus, the problems associated with high-power, high-voltage switches are now shifted to low-voltage, longer switching intervals.

A second possibility is using combinations of the previous circuits in a single system. A parallel system would provide voltage gain, a subsequent series system would provide additional pulse compression, and a transmission line system could shape the pulse and yield even more pulse compression and pulse sharpening.

For repetitive operation of magnetic switches and systems, the primary switch recovery time, the reset and the recharge times determine the minimum interval between subsequent output pulses. The primary switch presents the largest unsolved problem for repetitive operation.

III. MAGNETIC SWITCHES

A. Switching Characteristics

A magnetic switch is basically a saturable inductor [Fig. 9(a)]. After the switch is closed at $t = 0$, the inductive back voltage is opposite and nearly equal to the source voltage until the flux of magnetic material in the inductor core is exceeded. During the time before saturation, a small amount of leakage or magnetization current passes to the load [Fig. 9(b)]. As the magnetic core flux (volt-sec) is exceeded, the ferromagnetic portion of the inductor back voltage drops to zero, and the increase in circuit current is limited only by the stray or remaining inductance in the circuit. Another way of viewing the magnetic switch is that the saturable inductor changes from a large impedance to a small impedance at saturation.

One important point shown by Fig. 9 is that a magnetic switch can support or hold off a dc voltage for a finite time determined by the flux (volt-sec) of the magnetic material in the switch. Thus, voltage must be aplied to magnetic switches in a pulse manner that requires a conventional switch at some point if a dc supply source is used.

The switching characteristics of laminated magnetic material shown in Fig. 10 may be compared to those of conventional switches (spark gaps, thyratrons, SCRs) shown in Fig. 11. The most obvious differences are the voltage falltime and the minimum voltage during current conduction. The voltage fall of conventional switches decreases exponentially, and the conduction voltage drop is 40-200 V. In contrast, the back voltage of a magnetic switch falls linearly, not exponentially, and the conduction drop is determined by the resistance of the conductor carrying the current, which can be made very small. The only additional loss after switching is due to the core loss because eddy currents have ceased. The linear fall in magnetic switch voltage is due to the regenerative feedback of the saturation process, in which the saturation of one lamination increases the magnetic field drive to the remaining laminations causing the
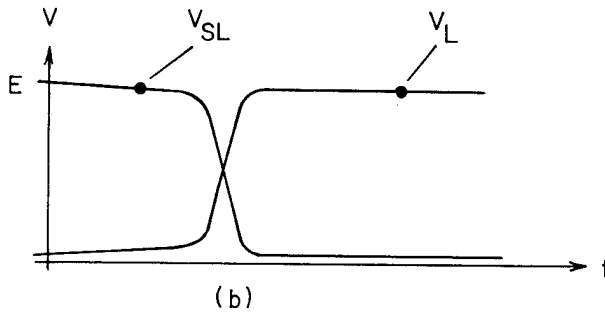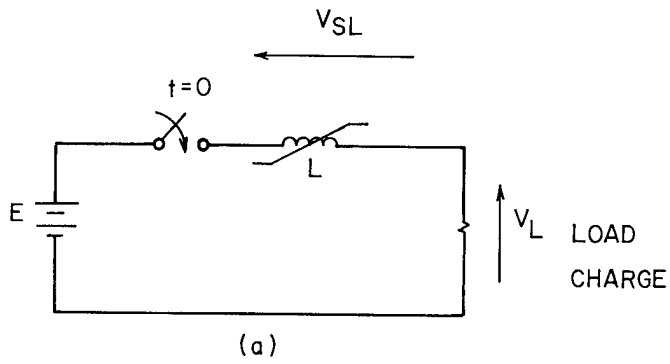
(a)

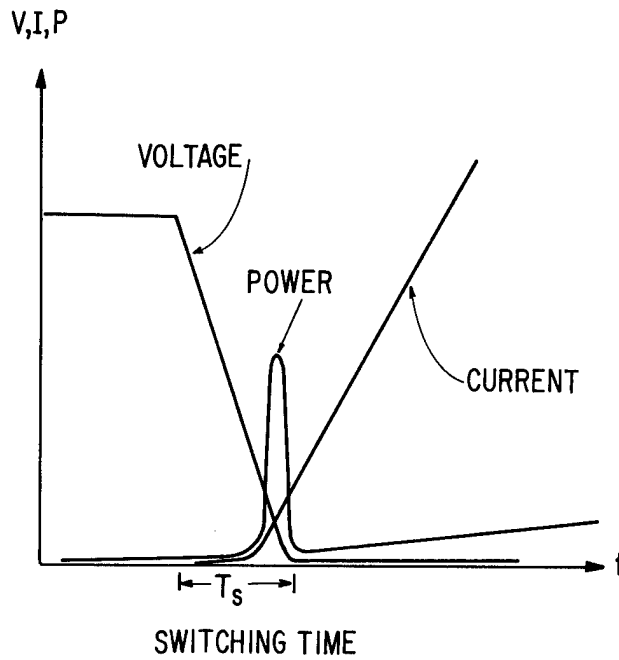Fig. 9.
Magnetic switch characteristics.

(b)

SWITCHING TIME
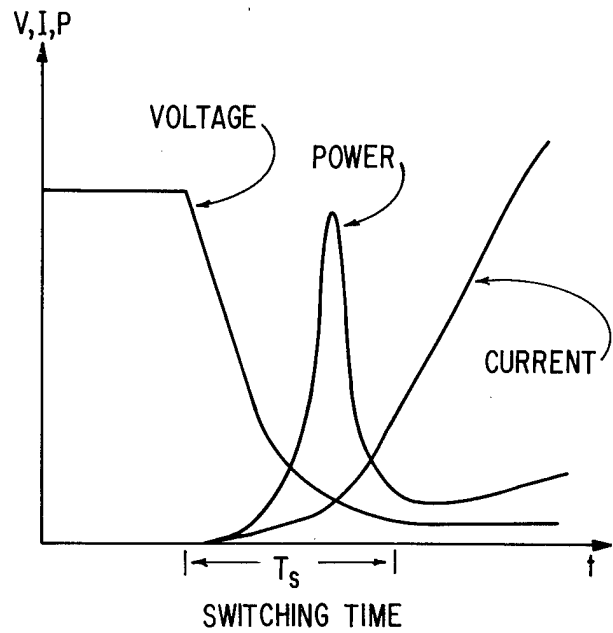
Fig. 10.
Magnetic switch waveforms.

SWITCHING TIME

Fig. 11.
Conventional switch waveforms.

next lamination to saturate faster, etc. As a result of magnetic switching, the rate of initial current rise is increased (compare Figs. 10 and 11), and the power dissipated in the switch is decreased because the switching time T_s is decreased.

B. Saturation Characteristics

In the low-voltage (10 kV) 1-10-μs pulse width range, the saturation process of the individual laminations is different from that for the high-voltage, short-pulse range. In the several microsecond, low-voltage range, the saturation process is gradual, and the relationship between the magnetic flux density (B-weber/m^2) and the driving magnetic field (H-Amp-Turns/m) observed externally (B-H curve) is proportional to the dc relationship for thin laminations (0.5-2 mil). The dimension factor, DF, of the magnetic material is defined as the ratio of the material skin depth δ to the lamination half thickness, 0.5 x_L

$$DF = \frac{\delta}{0.5x_L} = \left(\frac{\rho T}{\mu \, 2\pi}\right)^{1/2} \frac{2}{x_L} \quad . \tag{18}$$

Generally, for x_L of 0.0005 in., the value of DF is >1 for times or pulse widths t in the 10-μs range, ~ 1 for t = 1 μs, and <1 for t = 100 ns. The thinnest lamination that is somewhat cost effective in large quantities is 0.5 mil (1 mil = .001 in.). Thus, short-pulse (≤ 100 ns) magnetic switches operate in a region where the skin depth is much less than the material half thickness and a shock-like saturation wave exists in the material.

Figure 12 shows the spatial distribution of the major magnetic parameters when the skin depth is much less than the material half thickness. A steep saturation front propagates from the surface to the center of the lamination as the magnetic field increases at the lamination surface. In systems using saturated magnetic elements to generate short pulses, the driving surface field can be several orders of magnitude greater than the saturation field. Thus, the surface field rises to many times the saturation field before the saturation front, located at (x = X_f), can penetrate the lamination (Fig. 12). The local magnetic field in the lamination determines the local value of B. Thus, as the local magnetic field changes from zero to several times the coercive magnetic field H_c, the magnetic flux density changes from $-B_s$ to B_s, [Fig. 12(b)]. The penetration of the magnetic field into the lamination is resisted by the changing flux that drives eddy currents behind the saturation front. Because of uniform current distribution, the eddy-current magnetic field subtracts from the surface magnetic field linearly into the lamination so the net field is small at the saturation front.
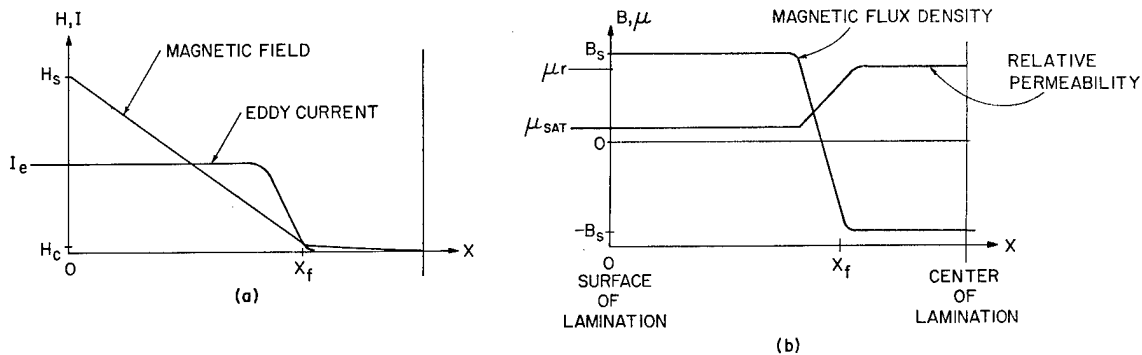

Fig. 12
Saturation parameter spatial distributions.

Several important observations emerge from Fig. 12. First, the relative permeability of the material behind the saturation front $\mu_{r\text{-sat}}$ where high magnetic field has penetrated, has a value from one to three, depending on the material and the overdrive conditions. The permeability of the material in front of the saturation wave, where the local field is small, has a relative permeability proportional to the dc value. The external circuit is affected by the region into which the magnetic field has penetrated or the region behind the saturation wave that changes as the wave progresses. The external circuit back voltage is determined by

$$V_B = -N \frac{d\emptyset}{dt} \tag{19}$$

and can be approximated by

$$\frac{d\emptyset}{dt} = \Delta B \frac{dA}{dt} \quad , \tag{20}$$

but

$$\frac{d\emptyset}{dt} \neq A \frac{dB}{dt} \quad . \tag{21}$$

In addition, the external circuit experiences an average inductance dependent upon an effective permeability that in turn is dependent on the saturation front position and velocity.

C. Interlamination Voltage

Fabrication of magnetic switches to handle large voltage is limited by the insulation between individual laminations. The cross-section area of magnetic material required to support a voltage waveform $V(t)$ is determined by conservation of flux or

$$\frac{1}{N_t} \int_0^{T/2} V(t)\, dt = \int_{A_m} \overline{B} \cdot \overline{d\,s} = 2B_{sat}A_m \quad , \tag{22}$$

where A_m is the area of the magnetic material and B_{sat} is the saturation flux density. For a resonant energy transfer system

$$V(t) = \frac{V_{max}}{2} (1 - \cos \omega t) \tag{23}$$

substitute Eq. (22).

$$\text{and } \frac{T}{2} = \frac{\pi}{\omega} \text{ yield} \tag{24}$$

$$\frac{1}{N_T} \int_0^{T/2} V(t) dt = \frac{V_{max}T}{4N_t} \quad , \text{resulting in} \tag{25}$$

$$A_m = \frac{V_{max}T}{8B_{sat}N_t} \quad . \tag{26}$$

In addition

$$A_m = N_L x_L W_L \quad , \tag{27}$$

where N_L is the number of laminations, x_L is the lamination thickness and W_L is the lamination width. If all the laminations have approximately the same length, the single turn voltage, V_{max}/N_T, is evenly distributed among N_L laminations so the interlamination insulation must withstand an interlamination voltage V_L given by

$$V_L \geq \frac{V_{max}}{N_T N_L} = \frac{8B_{sat}x_L W_L}{T} \left(\frac{SF}{1-SF} \right) \quad . \tag{28}$$

Commercially available magnetic cores made of thin laminations are usually useful for V_L at about 2 V. To fabricate short-pulse (50-500 ns), high-voltage (50-500 kV) magnetic switches, interlamination insulation must withstand voltages of about 50-100 V for lamination widths of ≥ 1 cm. To maximize the magnetic switching effect, the majority of the cross-section area in the magnetic switch must be magnetic material. The ratio of A_m to A_T, also containing insulating material, is defined as SF in Eq. (15). Thus, the insulating material must support an electric field E_I given by

$$E_I = \frac{V_L}{x_I} = \frac{8B_{sat}W_L}{T} \left(\frac{SF}{1-SF} \right) \quad . \tag{29}$$

where x_I is the insulation thickness.

For SF of ~ 0.8 and x_L of 0.5 mil, the insulation thickness is ~ 0.1 mil. An average breakdown electric field stress >300 V/mil is required in the interlamination insulation. In addition, the insulation must withstand the temperature needed by the magnetic material annealing cycle.

D. Switching Material Considerations

The relationship among material and geometrical parameters and the voltages, the currents, and the losses observed in the external circuit emerges from the following analysis.

The switching time or the back voltage falltime is the time required for the entire core to saturate. The magnetic back voltage begins to fall when the first lamination saturates and reaches zero when the last lamination saturates. For high-voltage, short-pulse applications, the magnetic material is driven many times past saturation. The velocity $\dot{X}_f$ and position X_f of the shock-like saturation wave are related to the material resistivity ρ and the surface magnetic field $H_s(t)$ by[4]

$$X_f(t)\dot{X}_f(t) = \frac{\rho}{\Delta B} H_s(t) \quad . \tag{30}$$

From Eq. (30) as the velocity can be determined as

$$\dot{X}_f(t) = \frac{1}{2} \left(\frac{2\rho}{\Delta B} \right)^{1/2} \frac{H_s(t)}{\left(\int_0^t H_s(y)dy \right)^{1/2}} \quad . \tag{31}$$

The surface driving field for each lamination depends on the magnetic path length. The surface field for the inside lamination, which is the minimum lamination length, is

$$H_s(t) = \frac{I(t)N_T}{\ell_{min}} \quad .$$

(32)

The time to saturate the inside lamination, $T_{sat\ min}$, is one-half x_L divided by the velocity of the saturation wave front or

$$t_{sat-min} = \frac{x_L \left\{ \int_0^t [I(y)/\ell_{min}]\,dy \right\}^{1/2}}{1/2(2\rho N_T/B_{sat})\,I(t)/\ell_{min}} \quad .$$

(33)

Similarly, the time for the outside lamination to saturate $T_{sat\ max}$ is given by

$$t_{sat-max} = \frac{x_L}{(2\rho N_T/\triangle B)^{1/2}} \frac{\left\{ \int_0^t [I(y)/\ell_{max}]dy \right\}^{1/2}}{I(t)/\ell_{max}} \quad .$$

(34)

Thus the voltage falltime is defined as the switching time T_{sw} and is the difference in $T_{sat\ max}$ and $T_{sat\ min}$ if the saturation of each lamination is independent, or

$$T_{sw} = \frac{x_L}{(2\rho/\triangle B)^{1/2}} \left(\ell_{max}^{1/2} - \ell_{min}^{1/2} \right) \frac{\left[\int_0^t I(t)dt \right]^{1/2}}{I(t)}$$

(35)

The falltime can be written as a magnetic switching factor (MSWF) or

$$T_{sw} = MSWF \frac{\left[\int_0^t I(t)dt \right]^{1/2}}{I(t)}$$

(36)

where

$$MSWF = x_L \left(\frac{B_{sat}}{\rho N_t} \right)^{1/2} \left(\ell_{max}^{1/2} - \ell_{min}^{1/2} \right) \quad .$$

(37)

Equation (37) demonstrates that the switching time is dependent on the difference in the square roots of the minimum and maximum magnetic paths. Thus, a tape-wound toroidal core with small inside diameter and much larger outside diameter has a long switching time. A toroid with inside and outside diameters approximately equal would have a much faster switching time.

Note that the MSWF can be approximated by

$$MSWF = t_L \left(\frac{B_{sat}}{\rho N_t} \right)^{1/2} 2\ell_a^{1/4} \left(\ell_{max}^{1/4} - \ell_{min}^{1/4} \right) \quad ,$$

(38)

where the average lamination length ℓ_a is defined by

$$\ell_a^{1/4} = \frac{\ell_{max}^{1/4} + \ell_{min}^{1/4}}{2} \quad .$$

(39)

The switching time should be kept as short as possible. MSWF includes the average magnetic path length and the difference in path lengths.

MSWF can be used to compare various switching materials. A commonly used switching material is 50% Ni-50% Fe sold under the trade names Deltamax* and Orthonol.** The 50-50 NiFe material with ρ of 50×10^{-8}, Ω/m can be fabricated as thin as 0.1 mil, but the more cost effective 0.5 mil is commonly used in critical applications. The newly developed amorphous steel material, Metglas,[†] is also a promising candidate because its resistivity is 2.5 times that of 50-50 NiFe. However, Metglas cannot be fabricated at reasonable cost with less than a 1.5-mil nominal thickness. Thus, the MSWF for 0.5-mil NiFe is slightly better than that for Metglas.

The above analysis involves a step magnetic flux distribution in the lamination as a first-order approximation. However, the thickness of the saturation front corresponds to the distance in which the magnetic flux density changes from $-B_s$ to B_s and can be approximated by

$$\Delta x_f = \frac{x_L}{2} \frac{M\,H_c}{H_{s\text{-max}}} \quad , \tag{40}$$

where $M\,H_c$ represents the required saturation magnetic field in multiples M of the coercive magnetic field and H_{s-max} is the surface magnetic field. This approximation is based on the linear decrease of the magnetic field from the surface of the lamination to the saturation front (Fig. 12). If the local relative permeability of the material is approximated by

$$\mu_r \simeq \frac{\Delta B}{\Delta H} \simeq \frac{2B_{sat}}{M\,H_c} \quad , \tag{41}$$

then the saturation front thickness is approximately

$$\Delta X_f \simeq \frac{x_L B_{sat}}{\mu_r H_{s\text{-max}}} \quad . \tag{42}$$

The time required for the saturation front to travel the additional distance ΔX_f at the time the saturation front reaches the center of the lamination is given by

$$t_{\Delta X_f} = \frac{\Delta X_f}{\dot{X}_f} \tag{43}$$

or

$$t_{\Delta X_f} = \frac{B_{sat} x_L}{\mu_r} \left(\frac{B_{sat}}{\rho} \right)^{1/2} \frac{\left[\int_0^t H_s(y)dy \right]^{1/2}}{H_s^2(t)} \quad . \tag{44}$$

The surface magnetic field $H_s(t)$ is dependent on the magnetic path length so that the additional saturation time between the inside and the outside laminations adds another term to MSWF, or

$$\text{MSWF} = x_L \left(\frac{B_{sat}}{\rho} \right)^{1/2} \left[\frac{B_{sat}}{\mu_r i(t)} \left(\frac{\ell_{max}^{3/2} - \ell_{min}^{3/2}}{N_t^{3/2}} \right) + \left(\frac{\ell_{max}^{1/2} - \ell_{min}^{1/2}}{N_t^{1/2}} \right) \right] \quad . \tag{45}$$

Equation (45) also points out the importance in reducing the switching time of a high permeability material, the magnetic material geometry, and the length differential.

E. Leakage or Magnetization Currents

Before saturation of the magnetic material, a leakage or magnetization current flows through the switch to the load. An optimum magnetic switch minimizes the presaturation leakage current and thus the analysis continues to determine leakage current parameter scaling. The surface magnetic field $H_s(t)$ driving the saturation wave front is related to the leakage current I_L by

$$H_s(t) = \frac{I_L(t) N_t}{\ell_a} \quad . \tag{46}$$

The back voltage induced in one lamination is given by

$$V_B = \frac{-d\emptyset}{dt} = -\frac{d}{dt} \int_A \overline{B} \cdot \overline{ds} \quad , \tag{47}$$

where $\emptyset$ is the magnetic flux. The magnetic flux density spatial distribution into the lamination in the x direction can be approximated as a step transition between $-B_{sat}$ and B_{sat} or

$$B(x,t) = B_{sat} \{ u(x) - 2u[x - X_f(t)] \} \quad , \tag{48}$$

where $X_f(t)$ is the position of the saturation front, B_{sat} is the saturation flux density, and $u(x)$ is the unit step function. Defining

$$ds = 2W_L dx \tag{49}$$

and completing Eq. (47) yields

$$V_B = -4W_L B_{sat} \dot{X}_f(t) \quad . \tag{50}$$

Assuming the voltages induced in each lamination are equal and the applied voltage V_{ap} is equal to the number of turns times the sum of the lamination back voltages, then

$$V_{ap}(t) = N_t N_L V_B(t) \quad , \tag{51}$$

where N_L is the number of laminations in the core and N_t is the number of conductor turns around the core.

Using Eqs. (31), (49), and (50), a relationship between the applied voltage and the leakage current can be determined such that

$$I_L(t) = \frac{1}{2} \left(\frac{x_L}{A_m} \right)^2 \left(\frac{1}{N_t} \right)^3 \left(\frac{\ell_a}{\rho B_{sat}} \right) V_{ap}(t) \int_0^t V_{ap}(t) dt \quad . \tag{52}$$

For a resonant charge waveform given by

$$V_{ap}(t) = \frac{V_{max}}{2}(1 - \cos \omega t) \quad , \tag{53}$$

where $T_{sat} = \frac{\pi}{\omega}$,

the leakage current at time T_{sat} has the form

$$I_L(T_{sat}) = \frac{1}{32}\left(\frac{x_L V_{max}}{A_m}\right)^2 \left(\frac{1}{N_t}\right)^3 \left(\frac{\ell_a}{\rho B_{sat}}\right) T_{sat} \quad . \tag{54}$$

The leakage current for the resonant charge transformer as seen across the magnetizing inductance is similar in form to Eq. (54).

The leakage current for an intertransmission line magnetic switch depends on the pulse shape propagating down the line. If the voltage pulse is trapezoidal and the switch is designed to saturate at maximum voltage, the voltage driving the leakage current is given by

$$V_{ap}(t) = 2V_{max}\frac{t}{T_r} \quad , \quad 0 < t < T_r \quad , \tag{55}$$

where T_r is the voltage risetime and the voltage doubles at the large impedance of the unsaturated switch. Then the leakage current for a ramp applied voltage is

$$I_L(t) = \frac{1}{2}\left(\frac{V_{max}x_L}{A_m T_r}\right)^2 \left(\frac{1}{N_t}\right)^3 \left(\frac{\ell_a}{\rho B_{sat}}\right) t^3 \tag{56}$$

for $0 < t < T_r$.

The leakage current scales as the lamination thickness squared. Therefore, a prime design specification for small leakage currents is minimum lamination thickness.

F. Eddy Current and Core Losses

The application of voltage across the saturable magnetic element generates a magnetic field, related to the leakage current by Eq. (46), that diffuses into the laminations. The conducting magnetic material resists the magnetic field penetration through induced eddy currents generated by the back voltage.

The eddy current $i_e(t)$ for an average magnetic path length ℓ_a can be determined from Ampere's circuital law or

$$\oint \overline{H} \cdot \overline{d\ell} = I\,N_t \quad , \tag{57}$$

where N_t is the number of conductor turns around the magnetic material. This yields

$$[H_s(0,t) - H(0.5x_L,t)]\ell_a = i_e(t) \quad , \tag{58}$$

where $H_s(0,t)$ is the magnetic field at the lamination surface, and $H(0.5x_L,t)$ is the magnetic field at the center of the lamination, $x = 0.5x_L$. However, because the magnetic field equals zero at the lamination center until saturation occurs, the eddy current for ℓ_a can be approximated by

$$i_e(t) = H_s(0,t)\ell_a = N_t I_L(t) \quad . \tag{59}$$

Comparing Eqs. (46) and (59) indicates that the eddy current in each lamination is equal to the external circuit leakage current times N_t.

The approximate energy lost to the eddy-current process and to hysteresis can be determined by

$$E_e(t) = N_L \int_0^t i_e(y)V_B(y)dy = \int_0^t i_L(y)V_{ap}(y)dy \quad . \tag{60}$$

Equation (60) can be expanded using Eq. (51) to yield

$$E_e(t) = \frac{1}{8} \left(\frac{x_L}{A_m}\right)^2 \left(\frac{1}{N_t}\right)^3 \left(\frac{\ell_a}{\rho B_{sat}}\right) \int_0^t V_{ap}^2(s) \int_0^s V_{ap}(r)dr \cdot ds \quad . \tag{61}$$

The energy lost to eddy current scales directly as the square of x_L and as ℓ_a and scales inversely as ρ. Thus, a minimum practical lamination thickness of highly resistive magnetic material is desired for the optimum magnetic switch. As discussed above, the amorphous steels are approximately three times as thick as the cost effective 0.5 mil NiFe steels of similar cost. Thus, even though the resistivity of the amorphous steels is 2.5 times that of NiFe materials, the scaling of eddy current energy loss favors NiFe materials by a factor of 3.

The required volume of magnetic material V_m is given by

$$V_m = \ell_a A_m \quad , \tag{62}$$

where A_m is determined by the required voltage holdoff in Eq. (13) and ℓ_a is determined by the saturated inductance of the magnetic element, which is a fraction α of the total inductance required to transfer a specific energy given by Eq. (11); or

$$\ell_a \simeq 2\ell_{sat} = \frac{2\mu_0\mu_{sat}N_T V_{max}T_c}{\alpha SF\ L_T\ 8B_{sat}} \quad , \tag{63}$$

where T_c is the charge period of the magnetic switch prior to saturation. The time used in Eq. (11) is the discharge time of the magnetic circuit after saturation or T_d so that the volume of magnetic material becomes

$$V_m = \frac{\pi^2\mu_0\mu_{sat}E_T}{8\ \alpha SF\ B_{sat}^2} \left(\frac{T_c}{T_d}\right)^2 \quad . \tag{64}$$

The eddy-current energy loss per unit volume for an applied voltage of the form $(V_{max}/2)(1 - \cos\omega t)$ becomes

$$\frac{E_e}{V} = 1.8\ \frac{x_L^2\ B_{sat}^2}{\rho\ T_c} \quad , \tag{65}$$

where saturation occurs at $T_c/2$. The ratio of the eddy-current loss to the energy transferred with no losses is thus

$$\frac{E_e}{E_T} = 2.3 \frac{x_L^2 \mu_0 \mu_{sat}}{\rho \, \alpha \, SF} \frac{T_c}{T_d^2} \quad . \tag{66}$$

The scaling relationships for eddy-current energy loss, Eq. (61), indicate that thin laminations of magnetic material with a large resistivity are essential to reducing these losses. The ratio of eddy-current energy loss to the energy transferred by the switch decreases as V_{max} increases, but the ratio increases as the square of the discharge time decreases. Equations (64) and (65) indicate that the lamination thickness (which should be minimum) is the only variable available for reducing the energy loss ratio.

The other loss mechanism in magnetic switches is the core loss, which is the area enclosed by the B-H curve. Because the initial computer model results (see below) implies that the dc B-H curve can be used locally in the material, the maximum core loss per unit volume for one-half cycle transfer is given by

$$E_c = (2B_{sat}) \, (H_c) \quad , \tag{67}$$

where H_c is the coercive force. The flux relationship of Eq. (13) and the material volume of Eq. (64) can be used to determine the ratio of the core energy loss to the energy transferred with no losses, or

$$\frac{E_c}{E_T} = \frac{\pi^2 H_c \mu_0 \mu_{sat}}{4 \, \alpha \, SF \, B_{sat}} \left(\frac{T_c}{T_d} \right)^2 \quad . \tag{68}$$

This analysis does not treat the energy loss owing to spin relaxation damping. However, the eddy-current loss observed in basic experiments[5] is approximately 55% of the total energy loss, which includes spin-relaxation damping. Therefore, the expected total energy loss is about twice the eddy-current energy loss predicted by this first-order analysis. The core loss and the eddy-current loss can be designed as a small percentage of the total energy transmitted for the high-power, high-voltage, short-pulse magnetic switch systems if thin lamination of high-resistivity material is available. If the energy loss owing to spin-relaxation damping scales like the eddy current, then, in principle, the loss problem can be overcome.

G. Effective Impedance

In this mode of operation, the μ_r of the magnetic material, usually defined as

$$\mu_r = \frac{dB}{dH} \quad , \tag{69}$$

is valid only locally in the material. With the magnetic field distribution of Eq. (33), the total permeability of the material behind the saturation front is $\cong$ to the free space permeability, μ_0. In front of the saturation wave, the local value of μ_r is valid, but since the majority of the field has not penetrated into this area, the external circuit is not influenced by this material.

The effective resistance in the external circuit can be determined from

$$R(t) = \frac{V_{ap}(t) i_L(t)}{i_L(t)^2} \quad , \tag{70}$$

where the numerator represents the instantaneous power loss in the magnetic material, and the denominator is the square of the instantaneous external current. This can be written as

$$R(t) = \frac{2(A_m/x_L)^2 \; (\rho N_t^3 B_{sat}/\ell_a)^{1/2}}{\left[\int_0^t I(y)dy \right]^{1/2}}$$ (71)

using Eqs. (36), (44), and (31).

Similarly, the effective inductance can be determined by a volume integral

$$L(t) = \frac{1/2 \int_v B \cdot H \cdot dv}{1/2 \; i_L^2(t)} \quad ,$$ (72)

where H and B are assumed colinear, the numerator is the magnetically stored energy in the volume behind the saturation front, and the denominator is the square of the instantaneous external circuit current. The magnetic field decreases linearly into the lamination and is approximated by

$$H(x,t) = H_s(t) \left(1 - \frac{x}{X_f(t)} \right)$$ (73)

where x is the depth into the lamination. Thus, the effective inductance becomes

$$L(t) = \frac{(4A_m/X_L)\ell_a \int_0^{X_f} B_{sat}H_s(t)\{ 1 - [X/X_f(t)] \} \, dx}{i_L^2(t)}$$ (74)

Using Eq. (23) the apparent external inductance becomes

$$L(t) = \left(\frac{A_m}{X_L} \right) \left(\frac{\rho B_{sat}}{\ell_a} \right)^{1/2} N_t^{3/2} \frac{\left[\int_0^t i_L(y)dy \right]^{1/2}}{i_L(t)}$$ (75)

A voltage applied constantly during saturation creates a ramp current and maintains a constant inductance.

IV. SATURABLE STRIPLINE TRANSFORMER DESIGN

The design of a high-voltage, short-pulse, low-inductance saturable transformer is essential to the parallel magnetic pulse compressor system in which the primary switch can be operated at reduced voltage levels and to increase system reliability and lifetime. For these reasons a saturable transformer design is proposed.

A. Requirements for Saturable Transformer

Resonant energy transfer through a transformer is accomplished in the circuit of Fig. 13(a). If the transformer magnetizing inductance L_m is neglected, the circuit can be reduced to that of Fig. 13(c), indicating that the maximum energy transfer for a specific maximum voltage and a specific pulse length is inversely proportional to L_T.
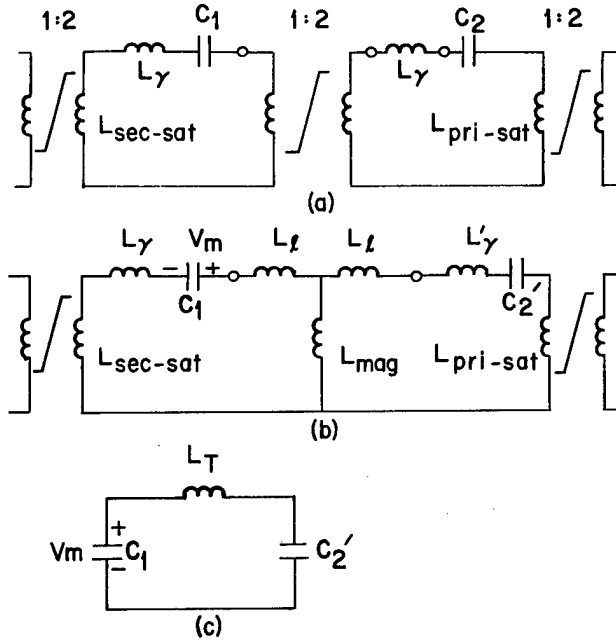
Fig. 13.
Transformer resonant energy transfer schematic.

Figure 13 labels:

1:2   C₁   1:2   C₂   1:2
L_γ L_γ
$L_{sec-sat}$ $L_{pri-sat}$
(a)

L_γ V_m L_ℓ L_ℓ L'_γ
C_1 C'_2
$L_{sec-sat}$ L_{mag} $L_{pri-sat}$
(b)

L_T
V_m C_1 C'_2
(c)

Figure 14 labels:

N_{pri} N_{sec}
I_1 K I_2
e_1 L_{pri} L_{sec} e_2

(a) BASIC TRANSFORMER SCHEMATIC

I_1 $(1-K)L_{pri}$ $(1-K)L_{pri}$ $I_2 \dfrac{N_{pri}}{N_{sec}}$
e_1 KL_{pri} $e_2 \dfrac{N_{sec}}{N_{pri}}$

(b) T- MODEL OF TRANSFORMER

$L_{pri-\gamma}$ $L_{pri-cap}$ $L_{pri}(1-K)$ $L_{pri}(1-K)$ $L_{sec-cap}\left(\dfrac{N_{pri}}{N_{sec}}\right)^2$ $L_{sec-\gamma}\left(\dfrac{N_{pri}}{N_{sec}}\right)^2$
$L_{sec-sat}$ C_{pri} KL_{pri} $C_{sec}\left(\dfrac{N_{sec}}{N_{pri}}\right)^2$
$L_{pri-sat}\left(\dfrac{N_{pri}}{N_{sec}}\right)^2$
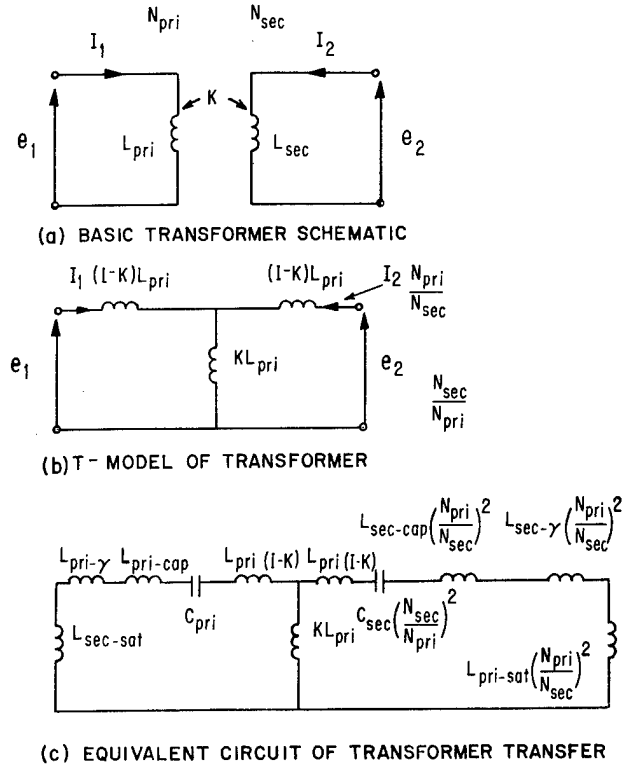
(c) EQUIVALENT CIRCUIT OF TRANSFORMER TRANSFER

Fig. 14.
Transformer equivalent circuits.

During the transfer of energy, the transformer can be analyzed like the basic transformer in Fig. 14. First, in Fig. 14(b), the transformer contributes inductance to the series path L_{ST}, so

$$L_{ST} = L_{pri}(1 - K) + L_{sec}\left(\frac{N_{pri}}{N_{sec}}\right)^2 (1 - K) \quad , \qquad (76)$$

where L_{pri} is the primary inductance, L_{sec} is the secondary inductance, N_{pri} is the number of primary turns, N_{sec} is the number of secondary turns, and K is the coupling coefficient. To minimize L_{ST}, to maximize the parallel magnetizing inductance L_{mag}, and to permit neglecting L_{mag}, the coupling coefficient must be as large as possible. Thus, maximizing the coupling coefficient is one important requirement for transformer design.

The decoupling of the saturated transformer prevents prepulses from reaching the load through the subsequent-stage transformers. Depending on the load prepulse requirements, the saturation coupling may be important to the design of the transformer system.

As the transformer saturates, the secondary back voltage begins to fall. As discussed in the previous section, the switching time or the back voltage time should be made as brief as possible to minimize the switch power dissipation. In addition, the switching time should be a small percentage of the total pulse width, and the magnetic geometry should be fast switching. Indeed, fast switching is the second important requirement for transformer design.

Following the transfer of the required energy by the transformer and the saturation of the transformer core causing the secondary back voltage to fall or switch, the sum of the stray inductance and the

saturated inductance of the magnetic material limits the current's rate of rise. The saturated inductance of the switch and that portion of the stray inductance in the secondary transformer must be minimized to obtain the short pulses desired. Thus a specific saturated inductance, usually very low, is the third important requirement for transformer design.

B. Low-Inductance Requirements

Excessive inductance is one of the major obstacles to obtaining short duration pulses in previous parallel magnetic pulse compressors. If the subsequent stage capacitances are matched through the coupling transformer turns ratio or

$$C_{sec} = \left(\frac{N_{pri}}{N_{sec}} \right)^2 C_{pri} \quad , \tag{77}$$

where C_{sec} is the secondary capacitance and C_{pri} is the primary capacitance; V_{sec} on C_{sec} is given by

$$V_{sec} = V_{pri} \left(\frac{N_{sec}}{N_{pri}} \right) \tag{78}$$

where V_{pri} is the maximum voltage on the primary capacitance. If the energy is to be transferred in half period $T/2$, then the total series inductance seen in the transformer primary is

$$L_T = \frac{1}{C_T} \left(\frac{T}{2\pi} \right)^2 = \frac{2}{C_{pri}} \left(\frac{T}{2\pi} \right)^2 \quad , \tag{79}$$

where

$$C_T = \frac{C_{pri} C_{sec} \ (N_{sec}/N_{pri})^2}{C_{pri} + C_{sec}(N_{sec}/N_{pri})^2} = \frac{C_{pri}}{2} \quad . \tag{80}$$

The total series inductance [Fig. 14(c)] in the primary of the unsaturated transformer $L_{pri\text{-}T}$ is

$$L_{pri\text{-}T} = L_{sec\text{-}sat} + L_{pri\text{-}\gamma} + L_{pri\text{-}cap} + L_{pri\text{-}leak} \quad . \tag{81}$$

When referred to the primary, $L_{sec\text{-}T}$ becomes $L'_{sec\text{-}T}$. The total inductance in the secondary of the unsaturated transformer $L_{sec\text{-}T}$ is given by

$$L_{sec}{}'_{-T} = \left(\frac{N_{pri}}{N_{sec}} \right)^2 (L_{pri\text{-}sat} + L_{sec\text{-}\gamma} + L_{sec\text{-}cap} + L_{sec\text{-}leak}) \quad . \tag{82}$$

The leakage inductances are proportional to the primary and secondary inductances related by

$$L_{sec} = \left(\frac{N_{sec}}{N_{pri}} \right)^2 L_{pri} \quad , \tag{83}$$

$$L_{pri\text{-}leak} = (1 - K)L_{pri} \quad , \tag{84}$$

and

$$L_{\text{sec-leak}} = (1-K)L_{\text{sec}} = (1-K)\left(\frac{N_{\text{sec}}}{N_{\text{pri}}}\right)^2 L_{\text{pri}} \quad . \tag{85}$$

If the capacitor and the stray inductances are assumed equal, or

$$L_{\text{pri-cap}} = L_{\text{sec-cap}} = L_{\text{cap}} \quad , \tag{86}$$

and

$$L_{\text{pri-}\gamma} = L_{\text{sec-}\gamma} = L_{\gamma} \quad , \tag{87}$$

all of the transformers have equal turn ratios such that the inductance of the previous transformer saturated secondary, $L_{\text{sec-sat}}$, is related to the inductance of the following transformer saturated primary, $L_{\text{pri-sat}}$, in magnitude by

$$L_{\text{sec-sat}} = \left(\frac{N_{\text{sec}}}{N_{\text{pri}}}\right)^2 L_{\text{pri-sat}} \quad . \tag{88}$$

Therefore, the total inductance becomes

$$L_T = 2L_{\text{sec-sat}} + (L_{\gamma} + L_{\text{cap}})\left[1 + \left(\frac{N_{\text{pri}}}{N_{\text{sec}}}\right)\right]^2 + 2\ (1-K)L_{\text{pri}} \quad . \tag{89}$$

Analytically, L_{pri} depends on the value of relative permeability for the magnetic material, which for high-voltage, short-pulse operation, is valid only locally in the material (see above). However, the saturated inductance of the transformer is given by

$$L_{\text{sat}} = \frac{\mu_o \mu_{\text{sat}} A_T N^2}{W_w} \quad , \tag{90}$$

where A_I is the insulator area and W_w is the width of the winding. The cross-section area is determined by the required flux content as in Eq. (13). Thus, the saturated inductance is determined by N and W_w. Because the saturated inductance or the switch inductance varies as the square of the number of turns and because voltage increase is desired, the number of turns used in a minimum inductance system is two. As a result, W_w is the only free variable.

This result is common to low-inductance system designs. Low inductance is usually achieved by using many separate conductors in parallel or by using one wide conductor or stripline. A coaxial transmission line whose radius is much larger than the separation between the inner and the outer conductors is also a low-inductance geometry and can be viewed as a stripline rolled on edge.

Choosing one of two magnetic geometries compatible with the stripline geometry determines the switching time.

C. Fast-Switching Magnetic Design

The back voltage falltime or the switching time is proportional to MSWF; from Eq. (37)

$$MSWF = x_L \left(\frac{B_{sat}}{\rho N_t} \right)^{1/2} \left(\ell_{max}^{1/2} - \ell_{min}^{1/2} \right) \quad , \tag{91}$$

where ℓ_{max} is the outside or longest magnetic path length and ℓ_{min} is the inside or shortest magnetic path length. To minimize the MSWF, the lamination thickness x_L is chosen as a small practical value based on cost and SF. The thinnest x_L available in the standard steels (about 0.25 mil) is expensive. One-half mil steel alloy tape is usually used as a compromise between cost and desired MSWF. The Metglas alloys are available only in thicknesses of 1-1.5 mils. MSWF depends inversely on the square root of ρ. The resistivity of Metglas materials is 2.5 times that of the NiFe steel alloys usually applied in high-frequency or switching applications. However, because Metglas is available only in 1.5-mil thickness, the 0.5 mil NiFe material MSWF is two-thirds that of the available Metglas MSWF for similar B_{sat} and tape geometry.

To minimize the difference in the magnetic path lengths, the tape material must be configured such that ℓ_a is much larger than the lamination stack height or

$$\ell_a \gg \frac{x_L \cdot N_{LS}}{SF} \quad , \tag{92}$$

where N_{LS} is the number of laminations in the stack.

If more magnetic material is required by Eq. (14), then several identical cores are placed side by side.

A composite design of a low-inductance, fast-switching transformer using strip transmission line and multiple fast-switching cores is shown in Fig. 15(a). This transformer can be used in the parallel magnetic pulse compressor Fig. 15(b). The multiple-core fast-switching magnetic design is directly applicable to a series switch or saturable inductor in a stripline (Fig. 2).

D. Transformer Coupling Design

The coupling coefficient of the saturable stripline transformer is the most important and most challenging part of the transformer design. The coupling coefficient should be as large as possible to reduce the effect of the shunt L_m [Fig. 14(c)]. Specifically, the magnetizing inductance should be designed so

$$L_{mag} \gg L'_{sec-T} \tag{93}$$

from Fig. 14(c) and Eq. (82), or

$$KL_{pri} \gg (L_{pri-sat} + L_y + L_{cap}) \left(\frac{N_{pri}}{N_{sec}} \right)^2 + (1 - K)L_{pri} \quad . \tag{94}$$

If $K \cong 1$ as desired, then

$$L_{pri} \gg (L_{pri-sat} + L_y + L_{cap}) \left(\frac{N_{pri}}{N_{sec}} \right)^2 \quad . \tag{95}$$

If the three inductances in Eq. (95) are the same order of magnitude, then

$$L_{pri} \gg 3 \left(\frac{N_{pri}}{N_{sec}} \right)^2 L_{pri\text{-}sat} \quad . \tag{96}$$

Using the identity for similar transformers,

$$L_{pri\text{-}sat} = \frac{\mu_{sat}}{\mu_\epsilon} L_{pri} \quad , \tag{97}$$

the requirements for the effective permeability μ_ϵ become

$$\mu_\epsilon \gg 3\mu_{sat} \left(\frac{N_{pri}}{N_{sec}} \right)^2 \quad . \tag{98}$$

The effective permeability can also be determined from the saturation wave-front formulation using the definition

$$L_{pri}(t) = \frac{\mu_0 \mu_\epsilon A_T N_{pri}^2}{\ell_a} \tag{99}$$

and Eq. (75) to obtain

$$\mu_\epsilon = \frac{L_{pri}(t)a}{\mu_o A_T N_{pri}^2} \quad , \tag{100}$$

or

$$\mu_\epsilon = \frac{2SF}{\mu_0 x_L} \left(\frac{\ell_a \, B_{sat}\rho}{N_{pri}} \right)^{1/2} \frac{\left[\int_0^t i(y)dy \right]^{1/2}}{i(t)} \quad . \tag{101}$$
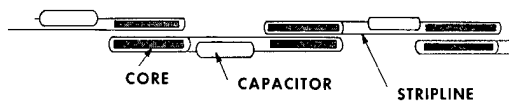
Characteristic values of the constants in Eq. (101) indicate that μ_ϵ will be much lower than that required by Eq. (98) for times of interest in the 50-100-ns range. Therefore, μ_ϵ cannot be used to increase the coupling coefficient between the transformer primary to total efficiency as desired.

To solve this problem a new approach to coupling the transformers primary and secondary is proposed. Because eddy currents limit the penetration of the magnetic field into the laminations, the magnetic field is forced to follow the lamination direction (Fig. 16). In this manner the magnetic flux is channeled from the transformer primary to the secondary if the magnetic field does not leave the area between the laminations. A conducting metal flux guide is proposed (Fig. 17) to force the magnetic field to remain between the laminations through the eddy currents induced in the guide, which may have to be made of a high-resistivity material such as stainless steel to reduce eddy-current losses. The flux guide could be made of metal similar to the tape-wound cores to prevent excessive eddy-current losses. In addition, to reduce the leakage inductance further, both the primary and secondary windings can be connected to the flux guide at one point to increase coupling.

A second alternative to the skin depth coupling method is the dual resonance transformer,[6] in which K = 0.6, and a bipolar output voltage transfers ~100% of the primary energy to the secondary. In the dual resonance transformer, the primary and secondary circuits are tuned to the same resonant frequency.
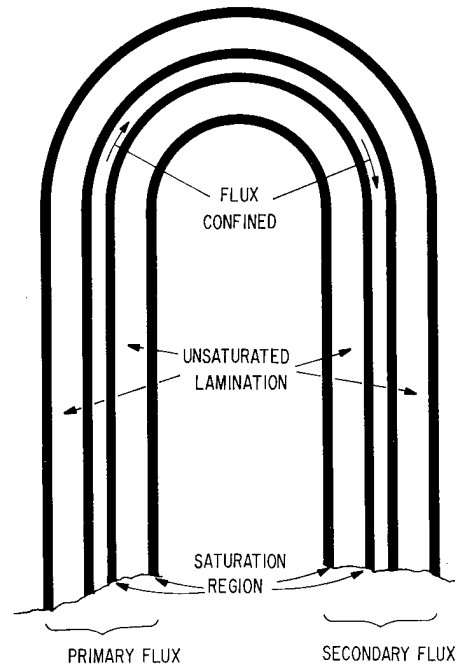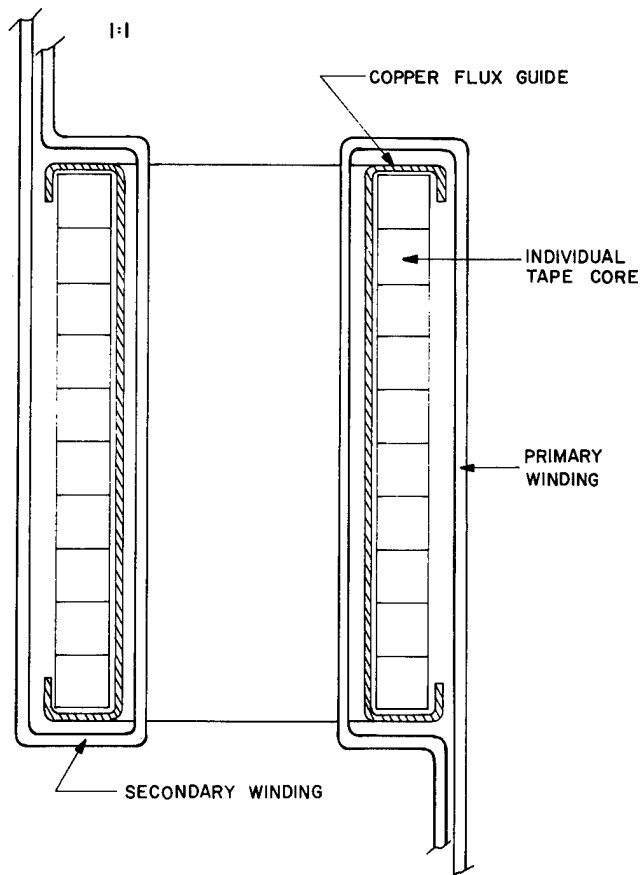
STRIPLINE MAGNETIC MODULATOR

SINGLE-TURN PRIMARY

2-TURN SECONDARY

MULTIPLE TAPE-
WOUND CORES
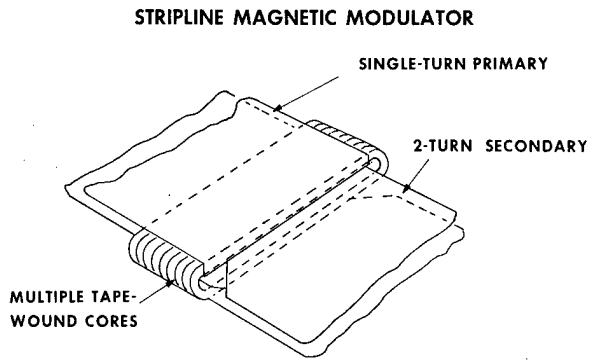
(a)   BASIC 1:2 SATURABLE STRIPLINE TRANSFORMER

CORE   CAPACITOR
STRIPLINE

(b)   SUCCESSIVE STAGE ARRANGEMENT

Fig. 15.
Fast-switching stripline transformer.

FLUX
CONFINED

UNSATURATED
LAMINATION

SATURATION
REGION

PRIMARY FLUX   SECONDARY FLUX

Fig. 16.
Illustration of presaturation flux coupling.

1:1

COPPER FLUX GUIDE

INDIVIDUAL
TAPE CORE

Fig. 17.
Skin-effect flux-guide illustration.

PRIMARY
WINDING

SECONDARY WINDING

V. COMPUTER SIMULATION

Several approximations of the saturation process in the magnetic material adequately describe the eddy-current loss and the major external effects such as current and back voltage. However, these approximations do not maintain credibility as the magnetic material passes through saturation. Therefore, a more detailed model of the saturation process has been developed to help in understanding the switching action of the magnetic material. The initial model simulated the saturable inductor and external circuit of Fig. 18. A later study will undertake a simulation of the saturable transformer.

The current I through the toroidal tape-wound magnetic core is related to the total induced back voltage V_{BT} (Fig. 18) by

$$\frac{dI}{dt} = \frac{V_c - V_{BT} - IR}{L_\gamma} \quad , \tag{102}$$

where V_c is the capacitor voltage, R is the circuit series resistance and L_γ is the circuit stray inductance. The capacitor voltage is also related to the current by

$$V_c = \frac{-1}{C} \int_0^t I \, dt + V_{max} \quad , \tag{103}$$

where V_{max} is the initial capacitor voltage and C is the capacitance.

The state equation for the circuit current, Eq. (102), illustrates the regenerative nature of the magnetic switching action. If one lamination saturates, V_{BT} decreases, the current derivative increases, and the surface magnetic field increases, driving the saturation of the remaining laminations through the relationship

$$H_s(t) = N_t \frac{I(t)}{\ell} \quad . \tag{104}$$

Because the length of each lamination increases with the radius in the toroidal core (Fig. 19), the surface driving magnetic field changes with radial position. This geometric effect results in a finite saturation time. To account for this factor in the simulation, the total number of laminations N_L making up the core cross section is divided into m groups such that each group has N_{Lg} laminations per group or

$$N_{Lg} = \frac{N_L}{m} \quad . \tag{105}$$

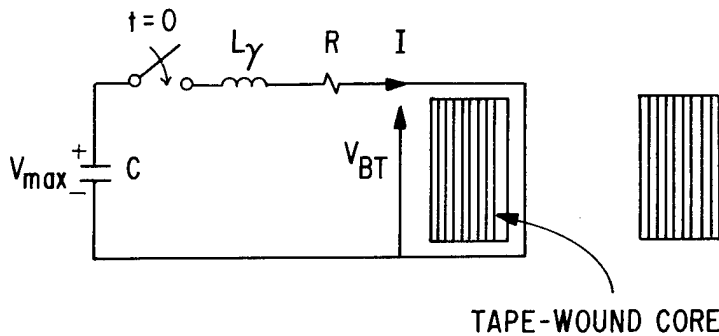
Fig. 18.
Saturable inductor simulation circuit.

The average length of a lamination for the mth group is then given by

$$\ell_{a,m} = 2\pi \left\{ R_I + \left[\frac{(m-0.5) N_{L_g} \cdot x_L}{SF} \right] \right\} \quad , \tag{106}$$

where R_I is the inside radius (Fig. 19). The driving field for the mth group of laminations is then

$$H_{s,m}(t) = \frac{I \cdot N_t}{\ell_{a,m}} \quad , \tag{107}$$

where $\ell_{a,m}$ is the average length of a lamination in group m.

The magnetic diffusion equation for each group of laminations is given by

$$\frac{dB_m(x,t)}{dt} = \rho \frac{d^2 H_m(x,t)}{dx^2} \tag{108}$$

and solved in time and space by assuming

$$\frac{dB_m}{dt} = \frac{dB_m}{dH_m} \cdot \frac{dH_m}{dt} \tag{109}$$

and writing finite difference state equations for the magnetic field at many points in the lamination (Fig. 20).

The relationship of B to H is determined locally from[7]

$$B(H) = \frac{B_{sat}(H + KS \cdot H_c)}{H_c \left(\frac{B_{sat}}{B_{rem}} - 1 \right) + (H + KS \cdot H_c)} - KB_k \tag{110}$$

where KS is ± 1; -1 if the right side of the B-H curve is used and $+1$ if the left side is used. The only variable in Eq. (110) is H because H_c, B_{sat}, and B_{rem} are all constants that can be determined experimentally. The term B_k is required as an offset constant if minor B-H loops are to be followed and is given by

$$B_k = \frac{1}{2} \left\{ \frac{B_{sat}(H_{max} + H_c)}{H_c[(B_{sat}/B_{rem}) - 1] + |H_{max} + H_c|} - \frac{B_{sat}(H_{max} - H_c)}{H_c[(B_{sat}/B_{rem}) - 1] + |H_{max} - H_c|} \right\} \quad , \tag{111}$$

where H_{max} is the maximum magnetic field amplitude. Differentiating Eq. (110) with respect to H yields a relationship for the relative magnetic permeability or

$$\frac{dB}{dH} = \frac{B_{sat} H_c (B_{sat}/B_{rem} - 1)}{\{H_c[(B_{sat}/B_{rem} - 1)] + (H + KS \cdot H_c)\}^2} \quad . \tag{112}$$
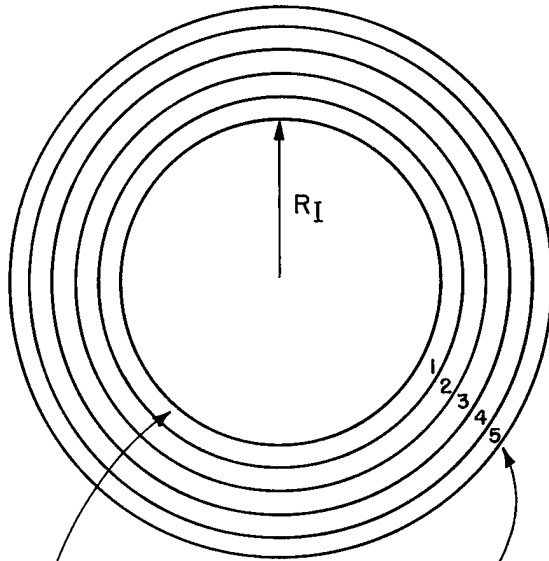
The total permeability is then modeled by adding μ_o to Eq. (112). The value of KS is determined from

$$KS = - \text{sign} \left(\frac{dI}{dt} \right) \quad . \tag{113}$$

LENGTH OF LAMINATION IN GROUP m

$$\ell_m = 2\pi \left(R_I + \frac{(m-0.5)N_{Lg}t_L}{SF}\right)$$

Fig. 19.
Simulation magnetic core.

NUMBER OF GROUP, m

N_{Lg} - LAMINATIONS PER GROUP

TOTAL NUMBER OF LAMINATIONS, $N_L = N_{Lg} \cdot m$
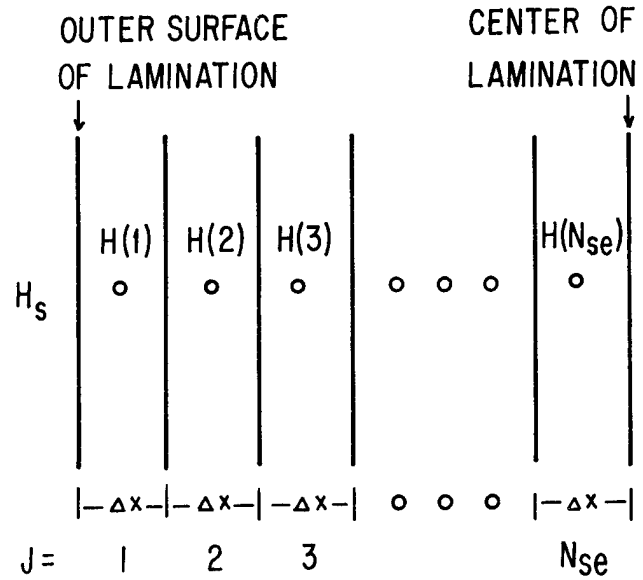
OUTER SURFACE OF LAMINATION   CENTER OF LAMINATION

Fig. 20.
Comuter simulation of lamination section.

The difference equations for the arrangement of Fig. 20 can be developed using Eqs. (108), (109), and (112). For the surface section, the difference equation is given by

$$\frac{dH(1)}{dt} = \frac{4\rho}{3(DX)^2} \frac{[2H_s + H(2) - 3H(1)]}{\left.\frac{dB}{dH}\right|_{H=H(1)}} \quad , \tag{114}$$

where the lamination half thickness is divided into N_{SE} sections of width DX such that

$$DX = \frac{x_L}{2N_{SE}} \quad . \tag{115}$$

The magnetic field difference equations for sections J where $J = 2$ through $N_{SE} - 1$ are given by

28

$$\frac{dH(J)}{dt} = \frac{\rho}{(DX)^2} \frac{[H(J-1) + H(J+1) - 2H(J)]}{\left.\dfrac{dB}{dH}\right|_{H = H(J)}} \quad .$$ (116)

For the section adjacent to the center of the lamination $J = N_{SE}$, the values of H in this section and the section on the other side of the center line are equal, or

$$H(N_{SE}) = H(N_{SE} + 1)$$ (117)

so that the difference equation for the inside section is

$$\frac{dH(N_{SE})}{dt} = \frac{\rho}{(DX)^2} \frac{[H(N_{SE}-1) - H(N_{SE})]}{\left.\dfrac{dB}{dH}\right|_{H = H(N_{SE})}} \quad .$$ (118)

The induced back voltage for a lamination in group m is determined from

$$V_{B,m} = N_T \frac{d}{dt} \int_A \overline{B_m} \cdot \overline{d s}$$ (119)

where the differential area ds can be defined as

$$ds = 2W_L dx \quad .$$ (120)

If the time derivative is moved inside the spatial integral and B is always perpendicular to x, then Eq. (119) becomes

$$V_{B,m} = - 2N_T W_L \int_{x=0}^{x = x_L/2} \frac{dB_m}{dt} \cdot dx \quad .$$ (121)

Further substitution of Eq. (108) gives

$$V_{B,m} = - 2N_T W_L \rho \int_{x=0}^{x = x_L/2} \frac{d^2 H_m}{dx^2} dx$$ (122)

or

$$V_{B,m} = - 2N_T W_L \rho \left. \frac{dH_m}{dx} \right|_{x=0}^{x = x_L/2} \quad .$$ (123)

Because the magnetic field is symmetrical about the center of the lamination,

$$\left. \frac{dH}{dx} \right|_{x = x_L/2} = 0 \quad ,$$ (124)

and

$$V_{B,m} = -2N_T W_L \rho \left. \frac{dH}{dx} \right|_{x=0} \quad . \tag{125}$$

Thus, the back voltage for a lamination in the mth group is given by

$$V_{B,m} = -2N_T W_L \rho \, [H_{s,m} - H_m(1)] \quad . \tag{126}$$

The eddy current for a lamination in the mth group can be determined using Ampere's law as in Eq. (57) or for the simulation

$$I_{e,m} = \ell_{a,m} \, [H_{s,m} - H_m(N_{SE})] \quad . \tag{127}$$

The m groups of laminations require the solution of m diffusion equations simultaneously, and the total back voltage generated by the entire core is given by

$$V_{BT} = N_{Lg} \sum_{k=1}^{m} V_{B,k} \quad . \tag{128}$$

The total eddy current is given by

$$I_{eT} = N_{Lg} \sum_{k=1}^{m} I_{e,k} \tag{129}$$

and the total instantaneous power being dissipated by eddy currents is given by

$$P_{eT} = N_{Lg} \sum_{k=1}^{m} I_{e,k} \cdot V_{B,k} \tag{130}$$

from which the total energy lost to eddy currents in t can be determined by

$$E_{eT} = \int_0^t P_{eT} \, dt \quad . \tag{131}$$

Graphic results of a computer simulation using the Los Alamos Systems Analysis Program (LASAN)[8] to solve the previous equations for a toroidal tape-wound core are shown in Figs. 21-24. Figure 21 illustrates the total back voltage seen in the external circuit of Fig. 18. Figure 22 shows the external circuit current. The back voltage falltime is linear and ~5 ns (Fig. 21). The back voltage illustrates numerical noise that could be reduced by reducing the simulation time step. The spatial distributions of H and B in the laminations are illustrated in Figs. 23 and 24, respectively. The spatial distribution plots show the linear decrease in the magnetic field into the lamination, which indicates a uniform current density. The sharp change in B at the saturation wave front is similar to the step function assumed previously. Also, the spread in the saturation front position between the inside and the outside of the core is related to the total saturation time or the back voltage falltime seen in Fig. 21. Another consequence of the steep saturation front seen in Fig. 24 is that the saturation time of the individual lamination is the quotient of the saturation front thickness divided by the velocity of the saturation front.
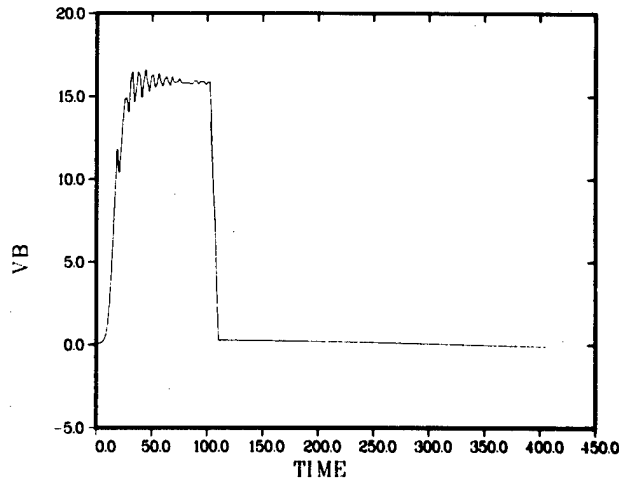
Fig. 21.
Back voltage for toroidal-core simulation.
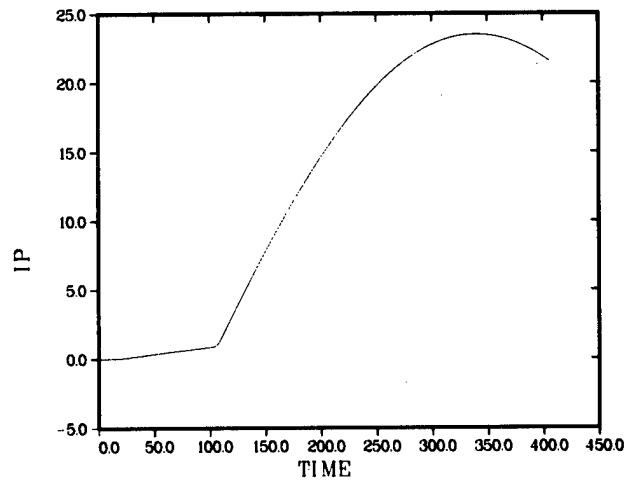
Fig. 22.
Circuit current for toroidal-core simulation.

SPATIAL DISTRIBUTION OF H AT TIME EQUAL   .75E+02

SPATIAL DISTRIBUTION OF B AT TIME EQUAL   .75E+02

LAMINATION PENETRATION (M)

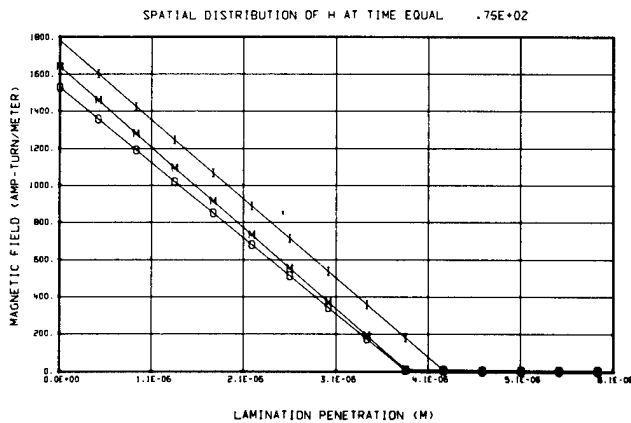LAMINATION PENETRATION (M)

Fig. 23.
Spatial distribution of H in core laminations. I is the value in
the inside lamination group; M is the value in the middle lami-
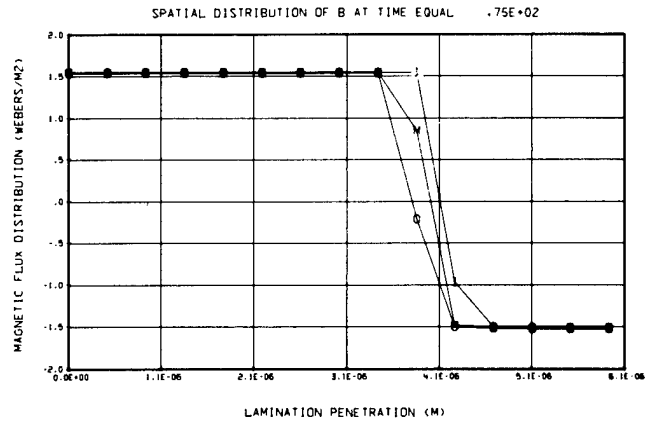nation group; O is the value in the outside lamination group.

Fig. 24.
Spatial distribution of B in core laminations.

Figure 25 illustrates the difference in leakage currents through a series saturable magnetic switch
before saturation for Metglas and NiFe materials. Figure 26 illustrates the energy loss owing to eddy
currents in the same circuit for Metglas and NiFe materials. Both of these results from the detailed
computer model agree with the first-order analytical model. Thus, the leakage current and the eddy-
current energy loss scale directly as the square of the lamination thickness and inversely as the material
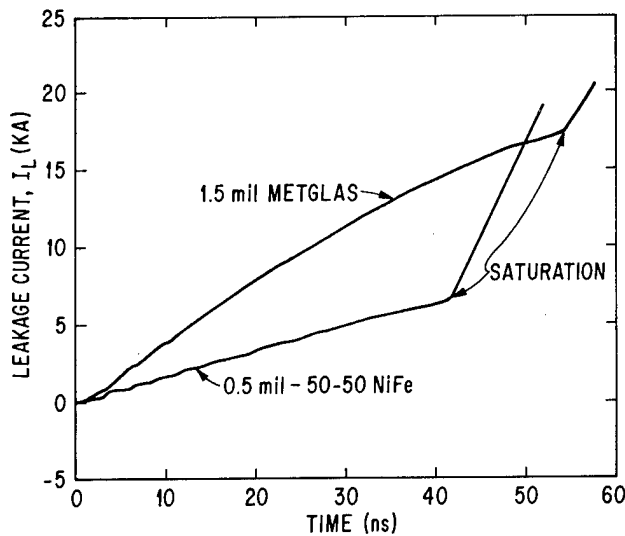resistivity.

Fig. 25.
Comparison of presaturation leakage currents for different materials.
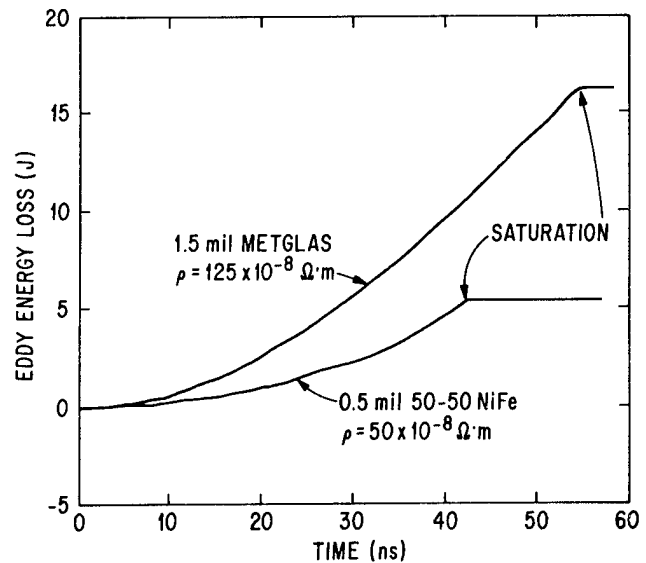
Fig. 26.
Comparison of eddy-current energy losses for different materials.

VI. PARALLEL MAGNETIC PULSE COMPRESSOR PRIMARY SWITCH

A. Requirements

Multiple magnetic pulse compression stages place the burden on the primary switch, which must be a conventional unit. For the parallel magnetic pulse compressor circuit, the primary switch may be solid state. That is why the parallel design using saturable transformers is desirable. If sufficient magnetic stages are used, primary solid-state switches do not have to be used in series but must switch a large current.

If the parallel magnetic system has no losses and the transformers have a voltage step-up ratio of two per transformer with equal inductances per stage, the primary switch requirements can be approximated. For n magnetic stages the maximum nth stage voltage V_n is related to V_{max} by

$$V_n = 2^n V_0 \quad . \tag{132}$$

To conserve energy, the nth stage capacitance C_n is

$$C_n = \frac{C_0}{2^{2n}} \quad , \tag{133}$$

where C_0 is the initial stage capacitance. If the series inductances for each stage are equal, then the resonant period of the nth stage T_n is

$$T_n = \frac{T_0}{2_n} \quad , \tag{134}$$

where T_0 is the resonant period of the initial stage.

32

The ratio of the peak current in the primary stage I_{pri} to the nth stage I_n is given by

$$\frac{I_p}{I_n} = \left(\frac{V_0}{V_n} \right) \left(\frac{C_0}{C_n} \right)^{1/2} \quad , \tag{135}$$

or using Eqs. (132) and (133),

$$I_0 = I_n \quad . \tag{136}$$

Therefore, the primary switch must conduct the same output current but at lower voltage and for a longer period. If the output pulse is square, the sinusoidal primary stage current must be multiplied by $\sqrt{2}$.

B. Primary Switch Specifications Example

The output requirements for a laser power supply to be used in isotope separation are listed in Table I. The resultant primary switch requirements are also listed in Table I.

The values listed in Table I show the large demands on the primary switch. Present solid-state switches turn on with switching times of about 0.5 to 5.0 μs, the faster switches being lower current (100 A). The solid-state device voltage during switching is a decreasing exponential (Fig. 11). To switch the currents indicated by Table I in 3.2 μs requires an evaluation program to determine whether commercial device operation can be extended or other methods should be developed.

VII. SUMMARY

This report examines the operation of saturable magnetic circuits and the material dependencies of the magnetic system variables and losses. In addition it proposes solutions to the low-inductance

TABLE I

ISOTOPE SEPARATION LASER POWER SUPPLY
PARAMETERS USING PARALLEL MAGNETIC
PULSE COMPRESSORS

Parameter	Value
Output voltage	50.0 kV
Output current	100.0 kA
Output pulse length	100.0 ns
Repetition rate	10.0 kHz
Number of parallel magnetic stages	6.0
Primary switch current	100.0 kA
Primary switch voltage	1.6 kV
Primary switch pulse length	6400.0 ns
Peak system power output	5.0 GW
Average system power output	2.5 MW

requirements and to the problem of designing a saturable transformer with a large coupling coefficient but without a high effective permeability material in the frequency range desired. The following summary of the individual portions of the report points out several important conclusions.

A. Circuit Conclusions

1. Series Magnetic Pulse Compressor.

a. Pulse compression at constant voltage.

b. Best for low-inductance, short-pulse duty.

c. Primary conventional switch must operate at output voltage at desired repetition rate.

2. Parallel Magnetic Pulse Compressor.

a. Pulse compression at constant current.

b. Best for pulse compression with voltage gain.

c. Primary conventional switch must operate at output current but at low voltage at the desired system repetition rate.

d. Requires more complicated saturable transformer.

3. Transmission Line Magnetic Pulse Compressor.

a. Used for pulse compression and shaping.

b. Modification of series circuit.

4. General Conclusions.

a. Combination of circuits can be used.

b. Standard pulse transformer or dual resonance transformer can be used to obtain voltage.

B. Low-Inductance Circuit Design

1. A maximum total circuit inductance in each pulse compressor stage cannot be exceeded to transfer E_T at V_{max} in a resonant half period $T/2$.

$$E_T = \left(\frac{V_{max} T}{2\pi} \right)^2 \frac{1}{L_T} \quad . \tag{11}$$

34

2. Magnetic material cross section determined by flux conservation

$$A_m = \frac{1}{\Delta B N_t} \int_0^{T_{sat}} V_{ap}(t)dt \quad .$$

(14)

3. The only free variable available in obtaining low-saturated inductance is ℓ_{sat} from

$$L_{sat} = \frac{\mu_0 \mu_{sat} N_t^2 A_m}{SF \ell_{sat}} \quad .$$

(12)

Because μ_{sat} is ~ 1, N_t is limited to 1 or 2, and A_m is determined by flux conservation.

C. Magnetic Circuit Design

1. The switching time of a magnetic system scales as

$$MSWF = x_L \left(\frac{B_{sat}}{\rho N_t} \right)^{1/2} \left(\ell_{max}^{1/2} - \ell_{min}^{1/2} \right) \quad .$$

(37)

2. The presaturation leakage current through the switch scales as

$$I_L(t) = \frac{1}{8} \left(\frac{x_L}{A_m} \right)^2 \left(\frac{1}{N_t} \right)^3 \left(\frac{\ell_a}{\rho B_{sat}} \right) V_{ap}(t) \int_0^t V_{ap}(y)dy \quad .$$

(52)

3. The eddy-current energy loss scales as

$$E_e(t) = \frac{1}{8} \left(\frac{x_L}{A_m} \right)^2 \left(\frac{1}{N_t} \right)^3 \left(\frac{\ell_a}{\rho B_{sat}} \right) \int_0^t V_{ap}^2(s) \int_0^s V_{ap}(r)dr \cdot ds \quad .$$

(61)

4. The effective permeability scales as

$$\mu_e(t) = \frac{SF}{\mu_0 x_L} \left(\frac{\ell_a B_{sat} \rho}{N_t} \right)^{1/2} \frac{\left[\int_0^t i(y)dy \right]^{1/2}}{i(t)} \quad .$$

(101)

5. The dielectric strength requirements for the interlaminar insulation scale as

$$E_I \geq \frac{8 B_{sat} W_L}{T} \left(\frac{SF}{1 - SF} \right) \quad .$$

(29)

All the scaling relationships indicate that thin laminations of magnetic material with high resistivity are essential to magnetic switches in high-voltage, short-pulse operation both for series saturable switches and for saturable transformers. Also, the general scaling is proportional to x_L^2/ρ such that 0.5 mil 50% Ni-50% Fe gives approximately triple the performance that the currently available 1.5 mil 2605 SC Metglas gives. The total energy loss is approximately twice that calculated for eddy currents, assuming

that the spin-relaxation damping loss compares to basic experiments. If scaling holds, the loss problem can be solved with extremely thin laminations of high-resistivity material. The other important parameter is the magnetic path length, which is determined by the required inductance. However, the difference in the longest and the shortest magnetic path lengths can and should be reduced to provide faster back voltage fall or switching times.

VIII. CONCLUSIONS

Magnetic switching systems can be developed to provide multigigawatt, multikilohertz pulses through compression of lower power pulses generated by state-of-the-art conventional systems if these areas of research and development are pursued.

First, the development of low-inductance or low-impedance circuits is essential to delivering the required energy at a specific voltage in a specific pulse length. These systems must use very wide conductors to yield the extremely low inductance required. The required inductances are possible if the designs presented in this report are used.

Second, development of thinner steel magnetic materials with high resistivity is also essential to operation of magnetic switch systems in the short-pulse, high-voltage mode. At present, 0.5 mil 50% Ni-50% Fe material is approximately three times superior to the 1.5 mil 2605 SC Metglas, even though the Metglas resistivity is 2.5 times that of the 50-50 NiFe. The computer simulations and analytical study both indicate that the use of steel materials at parameters of 50 ns and 50-500 kV may be impossible because of eddy-current losses unless methods of fabricating thinner material can be developed. Although ferrite material can be used for the short-pulse switching medium, the ferrite volume required is 10 times greater than the corresponding steel volume. An amorphous steel (Metglas) thickness of 0.25 mil would be 10 times superior to 0.5-mil NiFe and would cut costs.

Third, development of a high-temperature insulating technology is essential to using NiFe materials until amorphous steel materials can be fabricated in thinner laminations. Though the annealing temperature of the amorphous steel materials (365°C) is compatible with an organic insulation (Kapton) that can easily be fabricated in the thickness desired and has the dielectric strength required, the use of NiFe materials at thicknesses of 0.25 mil or less may be required to reduce eddy-current losses and presaturation-leakage currents to a tolerable level. To use the NiFe materials, an insulating material that can withstand the annealing temperature (750°C) and that has a dielectric strength of 500 V/mil in thicknesses of 0.05 mil is needed.

The development of a saturable transformer for use in the parallel magnetic pulse compressor will permit using a solid-state primary switch. Such a switch offers the possibility of a completely solid-state system implying reliability and long life. The transformer must have good primary to secondary coupling during the saturation of the magnetic core material. Transformer coupling is hindered by the very low effective permeability of the material during the fast saturation process. This report proposes a skin-effect, flux-coupling scheme to produce a totally efficient coupler compatible with the high-voltage, short-pulse mode of operation.

The analytical scaling relationships developed in this report agree very well with the detailed computer model results. In addition, the computer model has been calibrated with a simple toroidal core test system. The analysis reveals that the x_L^2/ρ scaling of the loss mechanism and the $(x_L^2/\rho)^{1/2}$ scaling of the switching time must be minimized for optimum magnetic switch operation.

This study shows that magnetic switches and circuits can be developed to provide the multigigawatt, multikilohertz power pulses. The development of magnetic switches and circuits will require research and development programs in magnetic materials, insulation materials, low inductance circuit fabrication and solid-state switching mechanisms. Magnetic switching technology is perhaps the only method of providing the multikilohertz, multigigawatt power pulses required by Department of Defense and Department of Energy research and weapons programs.

REFERENCES

1. W. S. Melville, "The Use of Saturable Reactors as Discharge Devices for Pulse Generators," Proc. Institution of Electrical Engineers (IEE, London, England, 1951), Vol. 98, pt. 3, pp. 185-207.

2. G. T. Coate and L. R. Swain, Jr., *High Power Semiconductor-Magnetic Pulse Generators* (M.I.T. Press, Cambridge, Mass., 1966), research monograph 39.

3. R. A. Mathias and E. M. Williams, "Economic Design of Saturating Rector Magnetic Pulsers," Trans. Amer. Inst. Electr. Eng. in *Communications and Electronics* (AIEE, New York, 1955), Vol. 74. no. 18, pp. 169-179.

4. V. W. Wolman and H. Kaden, "Uber die Wirbelstrom Verzögerung Magnetischer Schaltvorgänge (On the Eddy Current Delay in Magnetic Switching Processes)," Zeitschr. f. techn. Physik, 13, no. 7, 330 (1932).

5. J. E. L. Bishop, "The Shape, Energy, Eddy Current Loss, and Relaxation Damping of Magnetic Domain Walls in Glassy Iron Wire," *IEEE Trans. Magn.* (IEEE, New York, 1978) Vol. MAG-13, no. 5, pp. 1638-1645.

6. E. Cook and L. Reginado, "Off Resonance Transformer Charging for 250-kV Water Blumelein,"in *IEEE Trans. on Electronic Devices*, 13th IEEE Conference on Pulse Power Modulators, Buffalo, New York, June 20-22, 1978 (IEEE, New York, 1979), Vol. ED-26, pp. 27-33.

7. D. L. Lockwood, R. I. McNall, Jr., and R. L. Haumesser, "Development of Lightweight Transformers for Airborne High Power Supplies," Thermal Technical Laboratory report AFAPL TR-76-102, pp. 48-59 (December 1976).

8. P. A. Secker, P. L. Rivera, K. Stroh, and P. G. Bailey, Los Alamos Systems Analysis (LASAN) Computer Code, Los Alamos Scientific Laboratory, September 1979.

Page Range	Domestic Price	NTIS Price Code	Page Range	Domestic Price	NTIS Price Code	Page Range	Domestic Price	NTIS Price Code	Page Range	Domestic Price	NTIS Price Code
001-025	$ 5.00	A02	151-175	$11.00	A08	301-325	$17.00	A14	451-475	$23.00	A20
026-050	6.00	A03	176-200	12.00	A09	326-350	18.00	A15	476-500	24.00	A21
051-075	7.00	A04	201-225	13.00	A10	351-375	19.00	A16	501-525	25.00	A22
076-100	8.00	A05	226-250	14.00	A11	376-400	20.00	A17	526-550	26.00	A23
101-125	9.00	A06	251-275	15.00	A12	401-425	21.00	A18	551-575	27.00	A24
126-150	10.00	A07	276-300	16.00	A13	426-450	22.00	A19	576-600	28.00	A25
									601-up	†	A99

†Add $1.00 for each additional 25-page increment or portion thereof from 601 pages up.